RSC Advances

PAPER

View Article Online
View Journal | View Issue

Cite this: *RSC Adv.*, 2025, **15**, 25776

Structure-based design, synthesis, computational screening and biological evaluation of novel pyrrole fused pyrimidine derivatives targeting InhA enzyme†

Deepshikha Singh,[a] Praveen M. Parkali,[a] Umme Hani,[b] Riyaz Ali M. Osmani,[c] Nazima Haider,[d] Jyothi Kumari,[e] Dharmarajan Sriram,[e] Christian Lherbet,[f] B. C. Revan Siddappa[g] and Sheshagiri R. Dixit*[a]

Received 29th April 2025
Accepted 25th June 2025

DOI: 10.1039/d5ra03004h

rsc.li/rsc-advances

In this study, a series of 12 novel pyrrolyl chalcones and 22 pyrrole-fused pyrimidine derivatives were synthesized with good yields. Structural characterization was performed using FT-IR, NMR, and mass spectrometry techniques. The antitubercular potential of these compounds was evaluated using the microplate alamar blue assay (MABA). Among the synthesized compounds, compound **4g** exhibited the highest potency, with a minimum inhibitory concentration (MIC) of 0.78 mg mL^{-1} demonstrating greater efficacy than the standard drug isoniazid. Several other analogues also showed moderate to good inhibitory activity. Selected compounds were further assessed for cytotoxicity using human lung cancer (A549) and normal RAW cell lines, revealing low toxicity profiles. Enzymatic assays indicated that compound **4g** achieved 36% inhibition of InhA at a concentration of 50 μM. Additionally, molecular dynamics simulations were conducted to analyze the stability of the protein–ligand complexes, suggesting that these compounds hold potential for future development as InhA inhibitors in the fight against MDR-TB.

1. Introduction

Tuberculosis (TB) remains a leading cause of infectious disease-related mortality globally, with *Mycobacterium tuberculosis* infecting millions annually.[1] In 2023 alone, over 10.8 million new TB cases and approximately 1.25 million related deaths were reported, surpassing even COVID-19 in prevalence.[2] The growing emergence of multidrug-resistant (MDR-TB) and extensively drug-resistant (XDR-TB) strains has significantly hindered global eradication efforts.[3] The World Health Organization (WHO) has set ambitious targets to reduce TB mortality by 95% by 2035.[4] A critical barrier to effective TB management is the resistance of *M. tuberculosis* to first-line drugs such as isoniazid (INH), rifampicin, ethambutol, and pyrazinamide.[5] INH, a prodrug, requires activation by the KatG enzyme to inhibit enoyl-ACP reductase (InhA) depicted in (Fig. 1), a key enzyme in the fatty acid synthase-II (FAS-II) system essential for mycolic acid biosynthesis and bacterial survival.[6] However, mutations in KatG lead to resistance by preventing the activation of INH.[7] This has spurred interest in developing direct InhA inhibitors that bypass KatG and target the enzyme more selectively.[8,9]

Recent studies have explored various chemical scaffolds as InhA inhibitors, including antimycobacterial drugs such as triclosan, diphenyl ether derivatives, arylamide, pyrrolidine carboxamide analogues, 4-hydroxy-2-pyridones, chalcones, triazoles, quinolines, pyrroles, and pyrimidines.[8,10–14] Chalcones, synthesized through aldol condensation, which is a precursor for the synthesis of many other biological compounds, is the end product of the process itself, which combines substituted aryl ketones with aromatic aldehydes[15] and it have shown promising pharmacological properties such as anti-bacterial,[16] anti-inflammatory,[17] anti-cancer,[18] osteoporosis activity,[19] anti-fungal,[20] anti-malarial,[21] anti-viral,[22] anti-allergic,[23] and estrogenic effects.[24] Pyrimidines, another biologically active class, exhibit broad antimicrobial,[25] anti-inflammatory,[26] as anti-

[a]*Department of Pharmaceutical Chemistry, JSS College of Pharmacy, JSS Academy of Higher Education and Research, Sri Shivarathreeshwara Nagar, Mysuru, Karnataka, 570015, India. E-mail: sheshagiridixit@jssuni.edu.in; Tel: +91 721107207*

[b]*Department of Pharmaceutics, College of Pharmacy, King Khalid University, Guraiger, Abha, 62529, Saudi Arabia*

[c]*Department of Pharmaceutics, College of Pharmacy, King Khalid University, Al-Faraa, Abha, 61421, Saudi Arabia*

[d]*Department of Pathology, College of Medicine, King Khalid University, Guraiger, Abha, 62529, Saudi Arabia*

[e]*Department of Pharmacy, Birla Institute of Technology and Science-Pilani, Hyderabad Campus, Jawahar Nagar, Hyderabad, Telangana, 500 078, India*

[f]*Université de Toulouse, CNRS, Laboratoire de Synthèse et Physico-Chimie de Molécules d'Intérêt Biologique (LSCPMIB), 118 Route de Narbonne, 31062 Toulouse Cedex 09, France*

[g]*Department of Pharmaceutical Chemistry, NGSM Institute of Pharmaceutical Sciences (NGSMIPS), Nitte (Deemed to be University), Mangalore, Karnataka, 575018, India*

† Electronic supplementary information (ESI) available. See DOI: https://doi.org/10.1039/d5ra03004h

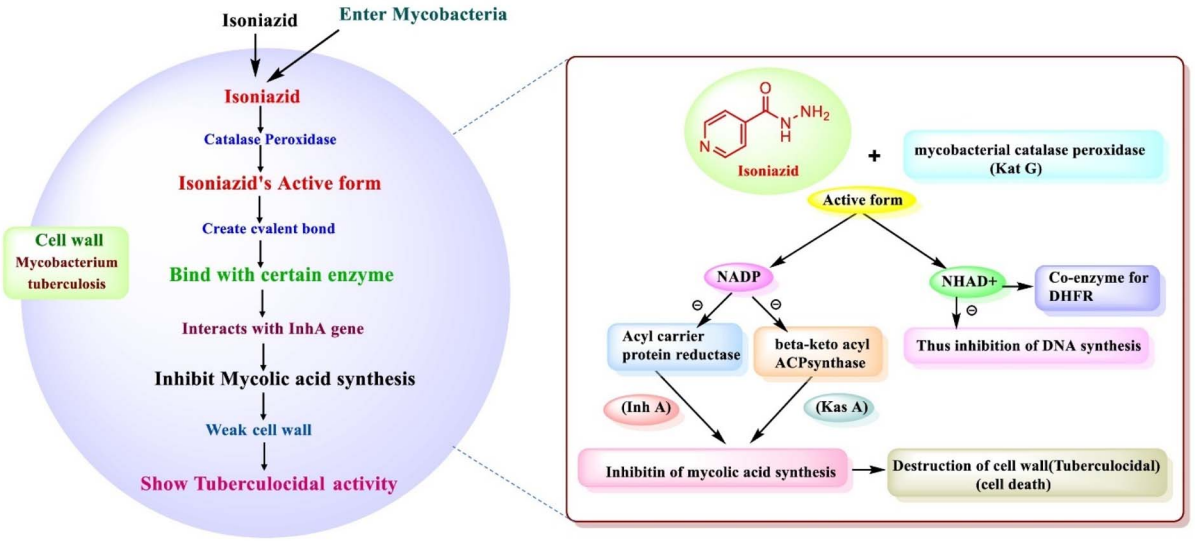

Fig. 1 Isoniazid-induced inhibition of mycolic acid synthesis.

tubercular[27,28] antibacterial agent & an anti-cancer agent.[29] Kaur *et al.* (2020) was investigated potential effectiveness of using pyrimidine derivatives as antitubercular drugs by several research organizations.[30] The maximum active compounds were examined used for their inhibition growth of *M. tuberculosis*.[31] According to literature survey we explore chalcones and pyrimidine derivatives found potential inhibitors against InhA. The combination of these motifs offers a promising strategy for novel therapeutic design.

Inha inhibitors are primarily used to treat tuberculosis due to their ability to improve and inhibit the tuberculocidal growth, but some studies have also suggested pyrimidines may have potential benefits in TB. In the framework of such research efforts, a pyrrole ring in the head region that is responsible for the activation. Our recent study aimed to design novel InhA inhibitors by replacing the aromatic ring structure with a pyrrole ring in the head region and aromatic trunk region for activation. Pyrimidine cyclization with aldehyde substitutions as electron withdrawing and donating group. With the understanding of the structural features of under clinical trial InhA inhibitors, such as acidic head, aromatic region with pyrrole ring, and lipophilic tail with pyrimidine ring and aromatic aldehyde substitutions a newer fragment focused library of molecules was designed (Fig. 2).

Pyrrole, a heterocyclic compound present in biomolecules like chlorophyll and heme, has also been widely studied for its antimicrobial activity. Its derivatives have demonstrated antitubercular efficacy both *in vitro* and *in vivo*, and compounds like (Sudoterb)LL3858 have progressed into preclinical development for TB.[32]

Based on these findings, the fusion of pyrrole, chalcone, and pyrimidine frameworks presents an attractive route for drug development.[33] Furthermore, several pyrimidine-containing compounds such as GSK2556286 and TBA-7371 are currently undergoing clinical trials for TB treatment depicted in (Fig. 3), showing efficacy without cross-resistance to current therapies. Similarly, SPR720, an oral antibiotic targeting bacterial DNA replication, is in clinical testing for mycobacterial infections.[34]

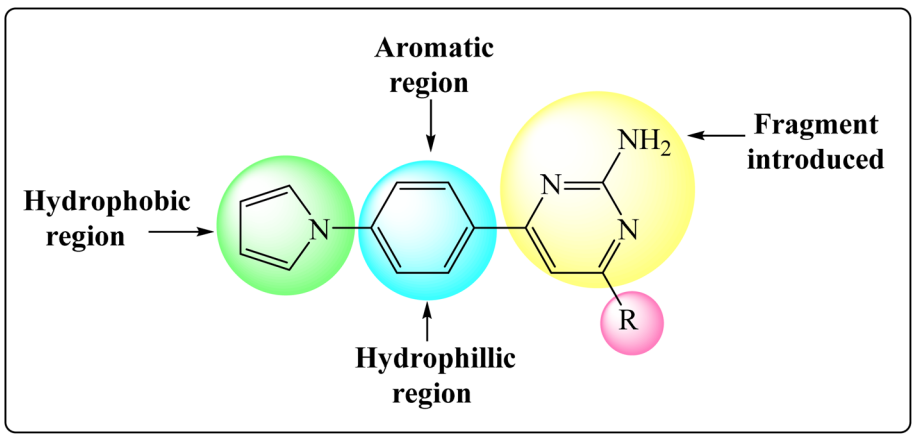

Fig. 2 Designed InhA inhibitors based on the structural features of InhA inhibitors.

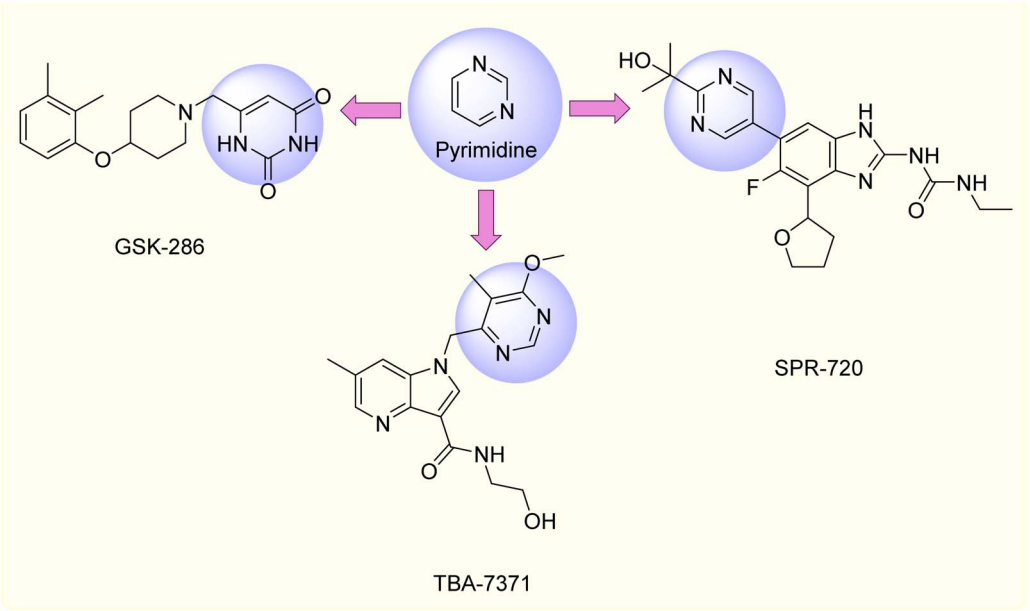

Fig. 3 Pyrimidine based *anti*-tb drugs candidate under clinical trials.

In our study, we report the design, synthesis, and biological evaluation of a series of novel pyrrolyl chalcones and pyrimidine-fused pyrroles. Their antitubercular potential was assessed through *in vitro* assays, cytotoxicity studies, enzyme inhibition activity, and molecular docking and dynamics simulations, with the aim of identifying effective and safe inhibitors of InhA.

2. Results and discussion

2.1 Rationale of molecular design

The novelty of this work highlights in presenting a pioneering approach through the design and synthesis of a new class of pyrrole-fused pyrimidine derivatives as potential inhibitors of the enoyl-ACP reductase (InhA) enzyme, a validated drug target involved in the biosynthesis of mycolic acids essential for bacterial survival, by development of a unique chemical scaffold, pyrrole-fused pyrimidines remain largely unexplored in the context of InhA inhibition. The rational design of these hybrid molecules introduces structural diversity and expands the chemical space for anti-tubercular drug discovery. Employing structure-based drug design strategies, including molecular docking and molecular dynamics simulations, the study effectively validates the binding affinity and potential inhibitory mechanism of the compounds against the InhA enzyme.[35]

2.2 ADME prediction and drug-likeness evaluation

The selected compounds were evaluated for their pharmacokinetic properties, including absorption, distribution,

Table 1 ADME score and toxicity profile[a]

S. no	Compound	#Stars	MW	Dipole	SASA	Donor H bond	Acceptor H bond	QPlog P_0/w	QPlog *S*	QPlog BB	No. of metabolites	QPlog khsa	% Human oral absorption
1	**3k**	1	315.41	0.00	658.09	0.000	2.000	5.890	−6.585	−0.242	1	1.172	100%
2	**3l**	1	279.35	0.00	569.92	0.000	2.000	4.920	−6.827	−0.019	1	0.676	100%
3	**4c**	0	372.42	0.00	372.42	2.000	2.000	4.858	−6.471	0.661	2	0.812	100%
4	**4g**	1	342.39	0.00	651.07	2.000	2.000	4.685	−6.105	−0.581	1	0.768	100%
5	**4h**	2	381.26	0.00	651.45	2.000	2.000	5.469	−7.047	−0.194	0	0.958	100%
6	**4u**	0	358.39	0.00	660.53	2.000	2.000	4.006	−5.670	−1.052	2	0.551	100%
7	**4k**	1	354.45	0.00	700.42	2.000	2.000	5.556	−7.231	−0.615	1	1.158	100%
8	Isoniazid	1	137.14	0.00	329.57	2.000	3.000	−0.646	−0.050	−0.840	2	−0.752	100%

[a] Key: #Stars: number of property or descriptor values that fall outside the 95% range of similar values for known drugs. A large number of stars suggests that a molecule is less drug-like than molecules with few stars. Dipole: computed dipole moment of the molecule. SASA: total solvent accessible surface area (SASA) in square angstroms using a probe with a 1.4 A radius. Donor H-bond: estimated number of hydrogen bonds that would be donated by the solute to water molecules in an aqueous solution. Acceptor H-bond: estimated number of hydrogen bonds that would be accepted by the solute from water molecules in an aqueous solution. QPlog $P_{o/w}$: predicted octanol/water partition coefficient. QPlog *S*: predicted aqueous solubility, log *S*. QPlog khsa: prediction of binding to human serum albumin, No. of metabolites: number of likely metabolic reactions. QPlog BB: predicted brain/blood partition coefficient. % Human oral absorption: predicted human oral absorption on 0 to 100% scale.

metabolism, and excretion (ADME), using the QikProp module of Maestro Schrodinger. This analysis was essential to assess their drug-likeness and biological significance. The results of the ADME prediction are summarized in (Table 1). All compounds displayed pharmacokinetic descriptors within the acceptable ranges for drug-like molecules, showing favourable comparisons with the standard anti-TB drug, isoniazid. Interestingly, isoniazid itself exhibited notable deviations in certain parameters, including molecular weight, drug-likeness, and predicted human oral absorption, when compared to the new compounds. Despite these deviations, all test compounds were predicted to possess favourable ADME profiles. The analysis suggests that further structural optimization (*e.g.*, derivatization) could lead to improvements in key parameters such as molecular weight, the number of hydrogen bond acceptors, predicted biological responses, blood–brain partition coefficient (QPlog, BB), and percent human oral absorption.[36] Among the tested compounds, **4c** and **4u** demonstrated the highest enhancement in drug-likeness, as reflected in their QikProp #star values, outperforming **4g** in terms of overall pharmacokinetic desirability. Therefore, after complete analysis of the structural features of available InhA inhibitors were designed, synthesized, analysed, and utilized in further *in vitro* studies. These results indicate their potential for further development as promising drug candidates against tuberculosis.

The synthesis of the compounds was initiated with the Paal–Knorr reaction of 4-aminoacetophenone and 2,5-dimethoxy tetrahydrofuran to yield (4-pyrrol-1-yl) acetophenone, which then underwent Claisen–Schmidt condensation with different substituted aldehydes to produce chalcones. These were subsequently cyclized with guanidine hydrochloride in sodium ethoxide and dry DMF to form pyrimidine derivatives. The final products were achieved after several rounds of refluxing, quenching, filtration, and column chromatographic purification.

This study focused on the development of novel pyrrole-based molecules, specifically 1-(4-(1*H*-pyrrol-1-yl)phenyl)-3-substituted prop-2-en-1-ones (Scheme 1) and 4-(4-(1*H*-pyrrol-1-yl)phenyl)-6-phenylpyrimidin-2-amines (Scheme 2), as

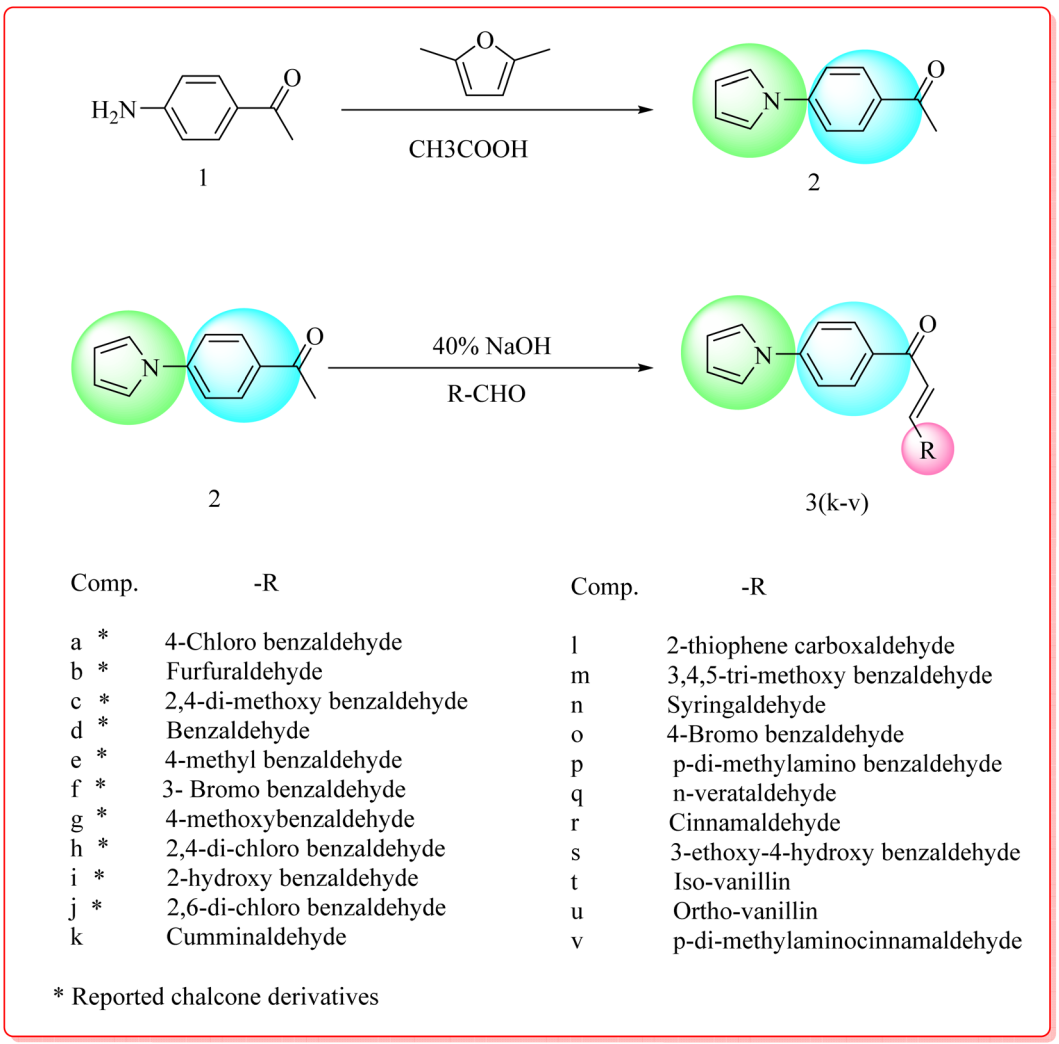

Comp.	-R	Comp.	-R
a *	4-Chloro benzaldehyde	l	2-thiophene carboxaldehyde
b *	Furfuraldehyde	m	3,4,5-tri-methoxy benzaldehyde
c *	2,4-di-methoxy benzaldehyde	n	Syringaldehyde
d *	Benzaldehyde	o	4-Bromo benzaldehyde
e *	4-methyl benzaldehyde	p	p-di-methylamino benzaldehyde
f *	3- Bromo benzaldehyde	q	n-verataldehyde
g *	4-methoxybenzaldehyde	r	Cinnamaldehyde
h *	2,4-di-chloro benzaldehyde	s	3-ethoxy-4-hydroxy benzaldehyde
i *	2-hydroxy benzaldehyde	t	Iso-vanillin
j *	2,6-di-chloro benzaldehyde	u	Ortho-vanillin
k	Cumminaldehyde	v	p-di-methylaminocinnamaldehyde

* Reported chalcone derivatives

Scheme 1 Synthetic route of a novel series of pyrrole chalcone derivatives.

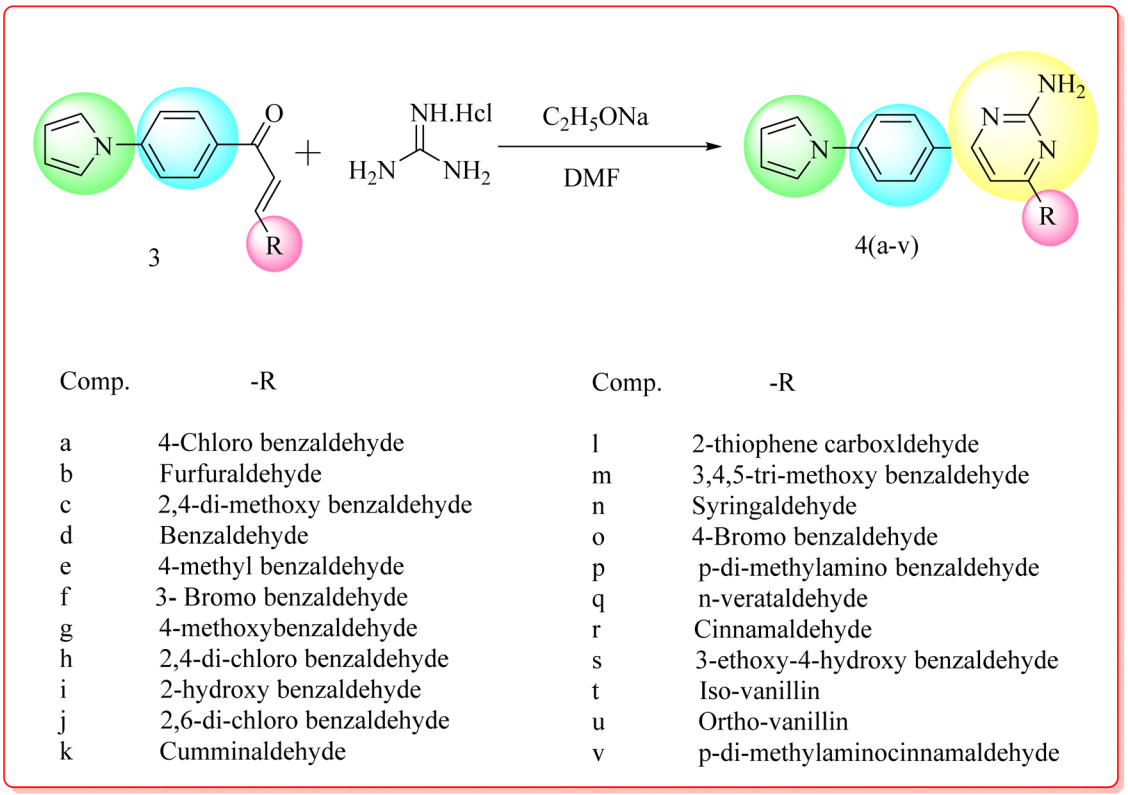

Comp.	-R	Comp.	-R
a	4-Chloro benzaldehyde	l	2-thiophene carboxldehyde
b	Furfuraldehyde	m	3,4,5-tri-methoxy benzaldehyde
c	2,4-di-methoxy benzaldehyde	n	Syringaldehyde
d	Benzaldehyde	o	4-Bromo benzaldehyde
e	4-methyl benzaldehyde	p	p-di-methylamino benzaldehyde
f	3- Bromo benzaldehyde	q	n-verataldehyde
g	4-methoxybenzaldehyde	r	Cinnamaldehyde
h	2,4-di-chloro benzaldehyde	s	3-ethoxy-4-hydroxy benzaldehyde
i	2-hydroxy benzaldehyde	t	Iso-vanillin
j	2,6-di-chloro benzaldehyde	u	Ortho-vanillin
k	Cumminaldehyde	v	p-di-methylaminocinnamaldehyde

Scheme 2 Synthetic route of a novel series of pyrimidine derivatives.

potential antitubercular agents. Biological evaluation against *Mycobacterium tuberculosis* H37Rv revealed that several compounds, notably **3k**, **3l**, **4c**, **4g**, **4h**, **4k**, and **4u**, demonstrated significant inhibitory effects. Among these, compound **4g** stood out with a minimum inhibitory concentration (MIC) of 0.78 μg mL^{-1}, indicating potent anti-TB activity. Cytotoxicity assessments using the A549 human lung cancer cell line showed that the most active compounds exhibited minimal toxicity, with cell viability remaining above 95% at tested concentrations. These results suggest that the synthesized compounds possess a favourable therapeutic index, supporting their potential for further pharmacological development.

InhA enzyme inhibition assays further supported the antitubercular efficacy of these compounds, with the same set of molecules displaying notable inhibition. Computational docking studies revealed favourable binding conformations within the InhA active site, including key hydrogen bonds and hydrophobic interactions, which likely contribute to their biological activity. These interactions were consistent with those observed for the reference drug isoniazid, strengthening the hypothesis that these compounds act as direct InhA inhibitors. To further substantiate these findings, MM-GBSA (molecular mechanics/generalized born surface area) calculations were performed to estimate the binding free energies of the ligand–enzyme complexes.[37] The calculated energies confirmed that the interactions were thermodynamically favourable, reinforcing the molecular docking results. Density functional theory (DFT) calculations were also carried out on the most promising compound, **4g**, which revealed a narrow HOMO–LUMO energy gap. This indicates high electronic reactivity and supports its potential for biological interaction. Additionally, molecular dynamics simulations conducted over 200 ns provided insight into the stability of the **4g**–InhA complex under physiological conditions. The complex remained stable throughout the simulation period, and analysis of the binding interactions identified key amino acid residues responsible for maintaining ligand–protein affinity. *In silico* ADMET predictions showed that the lead compounds adhered to Lipinski's rule of five and exhibited acceptable pharmacokinetic properties, suggesting good oral bioavailability and low toxicity risks. These findings highlight the drug-likeness of the synthesized molecules and their promise as lead scaffolds for further optimization.[38–44]

Overall, the combination of synthetic, biological, and computational approaches used in this study provides a solid foundation for the development of new antitubercular agents. The promising results, particularly for compound **4g**, warrant further investigations aimed at enhancing efficacy and selectivity, as well as exploring their mechanism of action in greater detail. These efforts may ultimately contribute to the development of effective, low-toxicity treatments targeting drug-resistant tuberculosis.

2.3 Molecular docking

A molecular docking study was conducted on InhA enzyme. The incorporation of carbon atoms into the respective mycolic acid demonstrates the involvement of the type II fatty acid

Table 2 XP docking studies of selected active compound among from the 34 compounds against the target InhA protein PDB-5OIR

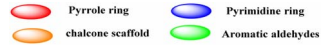

S. no.	Compound id	–R	Glide score (kcal mol^{-1})	Glide emodel score	Amino acid residue and hydrophobic, hydrogen and pi–pi interaction						
					Hydrophobic	Hydrogen	Pi–pi interaction	Positive	Negative	Halogen bond	Polar
1	**3k**	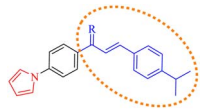	−7.794	−53.064	Met 98, Phe 97, Met 103, Phe 149, Met 155, Tyr 158, Met 161, Pro 193, Ala 198, Met 199, Ile 202, Ile 215, Leu 218,	—	—	—	—	—	
2	**3l**	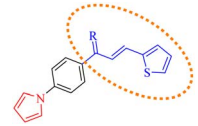	−7.697	−57.493	Phe 97, Met 98, Met 103, Phe 149, Tyr 158, Met 161, Ala 198, Met 199, Pro 193, Ile 202, Ile 215, Leu 218,	Tyr 158	Tyr 158	Lys 165	—	—	—
3	**4c**	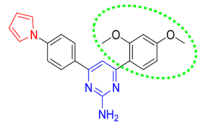	−6.623	−56.456	Met 98, Phe 97, Met 103, Phe 149, Tyr 158, Ala 198, Pro 193, Met 199, Ile 215, Leu 218	Gly 96	Tyr 158	—	—	Met 98	
4	**4g**	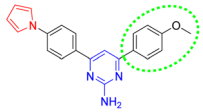	−8.911	−70.260	Phe 97, met 98, pro-99, Met 103, Phe 149, Met 155, Tyr 158, Met 161, Pro 193, Ile 194, Ala 198, Met 199, Ile 202, Ile 215, Leu 218,	Gly 96	—	—	—	—	Gln 100
5	**4h**	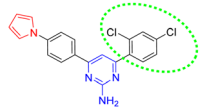	−7.947	−66.028	Phe 97, Met 98, Pro 99, Met 103, Ala 198, Phe 149, Tyr 158, Ile 194, Pro 193, Ala 198, Met 199, Ile 202, Ile 215, Leu 218	—	Tyr 158	—	—	—	Gln 100
6	**4k**	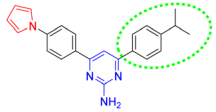	−8.470	−63.035	Phe 97, Met 98, Pro 99, Met 103, Met 103, Phe 149, Tyr 158, Pro 193, Ala 198, Met 199, Ile 202, Ile 215, Leu 218	Gly 96	Tyr 158	—	—	—	Gln 100
7	**4u**	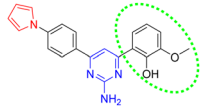	−7.947	−68.612	Phe 97, Met 97, Met 98, Pro-99, Met 103, Phe 149, Tyr 158, Pro 193, Ala 198, Met 199, Ile 202, Ile 215, Leu 218	Met 98	Tyr 158	—	—	—	Gln 100
8	Standard drug	Isoniazid	−4.160	−38.971	Met 103, Phe 149, Tyr 158, Met 161, Ala 198, Met 199, Ile 202	Tyr 158	—	—	—	—	

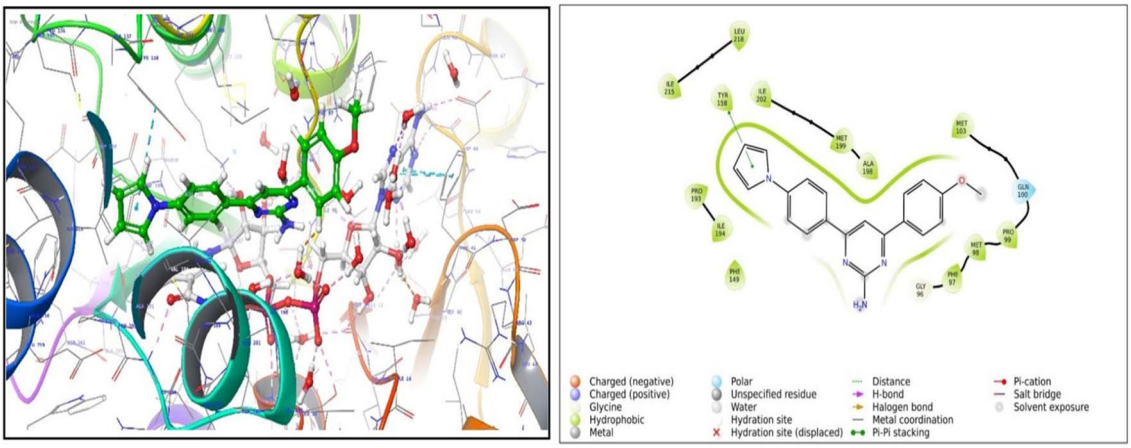

Fig. 4 (3D & 2D) interactions of compound **4g** with active site residues of the target protein PDB ID-5OIR.

biosynthesis pathway. MAs are a class of compounds known as long-chain alpha-alkyl beta-hydroxy fatty acids, C_{74} to C_{90}, and are the principal component of the mycobacterial cell wall which resists antibiotics and greatly increases mycobacterial virulency. Thus, the inhibition of InhA is considered one of the best ways to kill *Mtb* when it is both aerobic and anaerobic because of its lysis promoting action on cell walls, specifically on the mycolic acid that is crucial for the integrity of the mycobacterial cell wall.[45]

The inhibitors attach to InhA and interact with the enzyme's lipophilic binding pockets, tyrosine amino acid, and cofactor (NADH). InhA's binding pocket contains three significant sites where inhibitors interact. The catalytic site I comprises the tyrosine amino acid and the NAD cofactor's ribose group. Hydrogen bonds are established between the ribose ring of NAD and the active hydroxyl group of Tyr by suppressing its chain reaction. The structure of the inhibitor can determine the formation of bonds with methionine. Site II, which is a hydrophobic pocket, can be found near the side chain of Tyr and allows for the binding of hydrophilic components of inhibitors. Site III has a limited amount of research, with inhibitor rings located near NAD's phosphate groups and Gly 96 and Phe 97 at approximately the van der Waals distance.[46] These reported interactions of various ligands with the InhA enzyme show opportunities for designing new inhibitors that can attach to this area. In 2018, Prati *et al.* presented multiple crystal structures of new InhA NADH ligand complexes. One of them contains pyrimidine based co-crystallized ligand, which is obtained from the protein data bank (PDB ID: 5OIR),[47]check the interaction in between of protein & ligand by molecular docking study protocols. Docking results recommend that the developed compounds may serve as possible scaffolds for the development of anti-tubercular treatments. The glide score (kcal mol^{-1}) and glide emodel score, along with the interactions involving amino acid residues such as hydrophobic, hydrogen, and pi–pi interactions-indicate strong binding interactions between the protein and the all ligands, and with isoniazid used as the standard drug showing in below (Table 2).

We docked all compounds into the active pocket of InhA and identified their binding methods to the enzyme in order to support experimental anti-tubercular data and InhA inhibition data using computational approaches. The enzyme's binding affinity amino acid residues that interact with the all compounds include in ESI.†

Detailed intermolecular interaction between the ligands and protein was studied using glide docking. All compounds showed better docking scores compared to standard drug. Compounds **4h** and **4k** exhibited showed H-bonding interactions with the amine group, amides present at 5th position of pyrimidine ring and with Gly96 amino acid residue. Mostly all compounds showed pi–pi stacking interaction with Tyr 158 amino acid residue and **4u** compound showed the H-bonding interactions between OH group with Met 98 amino acid residue hydroxy group present at 2nd position of benzene ring, in compound **4l** showing H-bonding interactions between carbonyl group in bridging phenyl ring with Tyr 158 amino acid residue and pi–pi stacking interaction with thiophene ring.

Here, based on the biological activity data we focus on compound **4g**, which showed the most successful InhA inhibitors (Fig. 4). Displays the 2D, 3D image & spatial orientation and interaction patterns of compound **4g**.

2.4 MMGBSA

Here, the study was finalized to discover the free binding energies of the protein and ligand complexes using the (Molecular Mechanics, Generalized Born model and Solvent Accessibility). The complexes had their docking score (the lowest score) among all calculated and their optimal binding energy through prime module of Maestro Schrodinger software. OPLS-AA force field with electrostatics, such as the OPLS-AA force field was used for the analysis, in which the Vsbg 2.0 model employed a contained solvent model, and physics-based terms for pi–pi, hydrophobic interactions, and hydrogen bonding self-contact interactions were included in the present study. Docking was performed with the protein being static and ligands as stretchy.[37] The docked pose of ligand was rescored

Table 3 Hits identified after extra precision (XP) docking studies of selected active compound MMGBSA analysis was performed to investigate the free binding energies of the protein and ligand complexes

S. no	Compound IDs	MMGBSA-dG-binding energy	MMGBSA-dG-bind in coulomb	MMGBSA-dG-bind Co-valent	MMGBSA-dG-bind H bond
1	**3k**	−38.05	−1.33	9.75	−0.00
2	**3l**	−54.86	−18.17	5.25	−0.71
3	**4c**	−47.47	−12.94	6.36	−2.01
4	**4g**	−44.23	−7.99	9.85	−1.63
5	**4h**	−49.14	−7.81	7.34	−1.64
6	**4k**	−52.78	−14.78	10.77	−1.76
7	**4u**	−49.16	−9.46	6.44	−2.87
8	Isoniazid	−36.17	−33.93	0.15	−1.41

using MMGBSA process under prime module option in Schrodinger software showed in (Table 3).

The docking complexes were carried out using MM-GBSA calculation for the energy minimization of the protein–ligand complexes ($E_{complex}$), the free protein ($E_{protein}$), and the free ligands (E_{ligand}). The binding free energy ΔG_{bind} was determined according to the following equation:

$$DG_{bind} = E_{complex}(minimized) - E_{ligand}(minimized) - E_{receptor}(minimized)$$

3. Chemistry and synthesis

All compounds were synthesized as per steps outlined in Scheme 1 depicted in (Fig. 4). Condensation of 4-amino acetophenone (1) with 2,5-dimethoxytetrahydrofuran produced (4-pyrrol-1-yl) acetophenone (2) *via* the Paal–Knorr reaction. By using a sodium hydroxide catalyst to speed up the Claisen Schmidt condensation of (4-pyrrol-1-yl) acetophenone (2) with the substituted aldehydes in ethanol, the necessary critical intermediates, namely, chalcones (**3a–3v**), were produced. Chalcones (**3a–3v**) were cyclized to pyrimidine by reacting with Guanidine hydrochloride (0.007 mol) in the presence of sodium ethoxide (0.02 mol) and dried DMF (15 mL) as a solvent as depicted in Scheme 2 depicted in (Fig. 5). Reaction mixture was refluxed at 80 °C for 30–35 h, and reaction monitored by TLC. The reaction mixture was quenched with crushed ice, yielding a ppt solid which was filtered off, washed with water, hydrated and purified by column-chromatography (2 : 1), ethyl acetate and *n*-hexane. FTIR, ^{1}HNMR, ^{13}CNMR, and mass spectroscopy were used to confirm the structures of all the synthesized compounds. IR spectra of compound **3k**, peaks were observed at the carbonyl group from the α,β-unsaturated fragment was linked to an absorption band at 1657.65 cm^{-1} in the which is characteristic of the chalcone series (**3a–3v**). The presence of a methyl group is indicated by a singlet at *d* 1.23–1.22 ppm and doublets at *d* 7.96 and 8.26 ppm in compound **3k** ^{1}H NMR spectra. Two triplets were produced by the pyrrole moiety's protons at *d* 6.34 and 7.35 ppm, respectively. Compound **3k** ^{13}C NMR spectra revealed the signal at *d* 187.68 ppm. Every other aromatic carbon resonated within the anticipated *d* 111.56–143.98 ppm range. The synthesis of the needed product was confirmed by the molecular ion signal at *m*/*z* (M^+ + 1) 316.15. The amino group and C=N stretching at 1676.37 cm^{-1} are represented by the aromatic peak at 3320.38 cm^{-1} in compound **4g** IR spectra. Furthermore, two hydrogens were anticipated to be present at 5.25 (s, 2H) in the ^{1}H NMR spectra, which is related to the aromatic NH_2 group. Additionally, the mass spectrum supported this molecule by showing its molecular ion

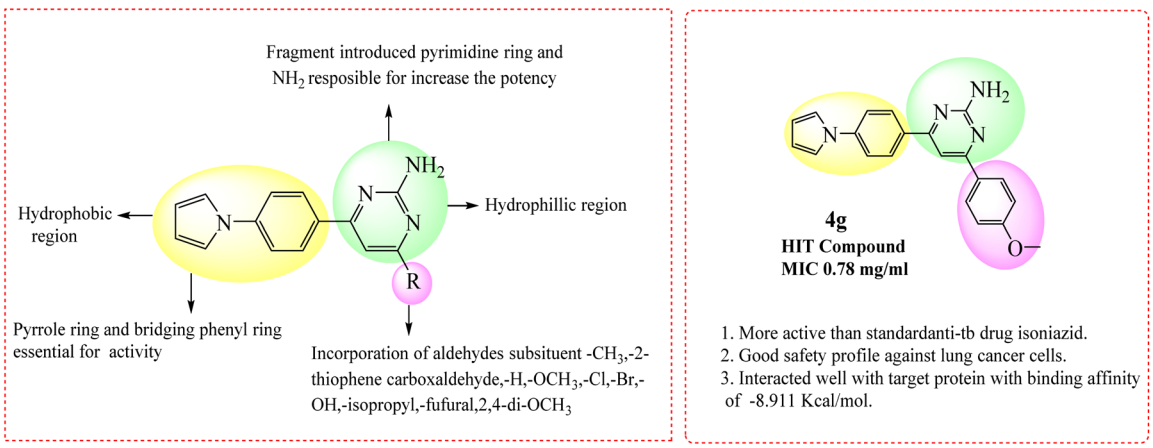

Fig. 5 SAR of pyrimidine derivatives and more active compound **4g**.

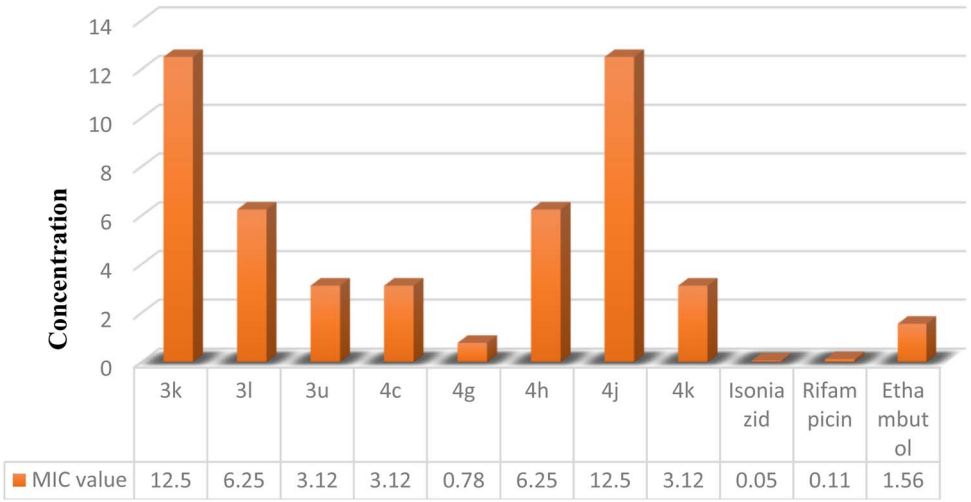

Fig. 6 Graphical representation of MIC for selected active compounds (MIC value range between 0.8 and 12.5 μg mL^{-1}).

Table 4 MABA assay to determine the MIC (minimum inhibitory concentration) of compounds against *Mycobacterium tuberculosis* $H_{37}Rv$

S. no.	Compound ID	MIC values (mg mL^{-1})
1	**3k**	**12.5**
2	**3l**	**6.25**
3	**3m**	>25
4	**3n**	25
5	**3o**	>25
6	**3p**	25
7	**3q**	>25
8	**3r**	>25
9	**3s**	>25
10	**3t**	>25
11	**3u**	**3.125**
12	**3v**	25
13	**4a**	>25
14	**4b**	25
15	**4c**	**3.125**
16	**4d**	**12.5**
17	**4e**	**12.5**
18	**4f**	>25
19	**4g**	**0.78**
20	**4h**	**6.25**
21	**4i**	>25
22	**4j**	**12.5**
23	**4k**	**3.125**
24	**4l**	>25
25	**4m**	>25
26	**4n**	>25
27	**4o**	25
28	**4p**	25
29	**4q**	>25
30	**4r**	**12.5**
31	**4s**	>25
32	**4t**	25
33	**4u**	>25
34	**4v**	25
35	Isoniazid	0.05 (μg mL^{-1})
36	Rifampicin	0.1 (μg mL^{-1})
37	Ethambutol	1.56 (μg mL^{-1})

peak at *m*/*z* (M^+ + 1) 343.14, which is in line with its molecular weight and validated the synthesis of the intended product.

3.1 Anti-tubercular activity

The described derivatives were examined for their anti-TB activity (Table 4). As a result of the preliminary anti-TB screening the most compounds own good activity. The activities of **3k**, **3l**, **3u**, **4c**, **4d**, **4e**, **4g**, **4h**, **4j**, **4k**, **4r** are expressed of minimum inhibitory concentration values, is shortcut by drugs: isoniazid, ethambutol, rifampicin. In series **3l**, **4h** compounds were active at MIC of **6.25** mg mL^{-1}, and better activity were shown with **3u**, **4c**, and **4k** compounds with MIC value of **3.125** mg mL^{-1}. Most active compound was **4g** is with a MIC value of **0.78** mg mL^{-1}. Better anti-tubercular activity was shown with this from the existence of biologically active hetero-aryl groups chalcone and aromatic ring link with pyrrole ring. The inhibitory activity of the pyrimidine derivatives was relatively higher than that of the chalcones. That's encouraging to observe that compounds **3u**, **4c** and **4k** was revealed with good anti-tubercular activity against tuberculosis MIC value **3.125** mg mL^{-1} while **4g** exhibited the capable activity MIC **0.78** mg mL^{-1}. Based on the study structure–activity relationship of the molecule depicted in (Fig. 5 and 6, Table 4).

Table 5 Cytotoxicity activity on normal cell line

S. no.	Comp. ID	% Toxicity at 25 μg mL^{-1}
1	**3k**	30.1
2	**3l**	26.6
3	**4c**	25.80
4	**4g**	19.09
5	**4h**	26.80
6	**4k**	28.90
7	**4u**	19.10
8	Isoniazid	0.05 (μg mL^{-1})

Table 6 Cytotoxicity activity on lung cancer cell line[a]

S. no.	Compound ID	IC_{50} (mM)
1	**4c**	55.12
2	**4g**	49.44
3	**4h**	104.77
4	**4k**	123.36
5	**4u**	123.36
6	Cisplatin	9.90

[a] IC_{50} – is half maximal inhibitory concentration-it is the half maximal (50%) inhibitory concentration (IC) of a substance (50% IC, or IC_{50}).

Table 7 Enzyme inhibition assay studies[a]

S. no.	Compound ID	Solubility	% inhibition InhA at 50 μM of inhibitor
1	**3k**	DMSO-d_6	36
2	**3l**	DMSO-d_6	36
3	**4c**	DMSO-d_6	16
4	**4g**	DMSO-d_6	36
5	**4h**	DMSO-d_6	<5
6	**4k**	DMSO-d_6	10
7	**4u**	DMSO-d_6	NI
8	Triclosan	DMSO-d_6	>99

[a] NI: for no inhibition.

3.2 MTT cytotoxicity studies

3.2.1 MTT-based cytotoxicity activity on normal cell line. Cytotoxicity was undertaken in the mouse macrophage cell line (RAW 264.7) with 25 μg mL^{-1} concentration. Subsequently 48 h of exposure, MTT metabolization stayed used to measure cellular viability by the cell production assay. The cells remained grown-up on T25 flasks with RPMI medium containing 10% FBS, penicillin at 10 000 units, and streptomycin at 10 mg per mL until attaining 80–90% confluency. The cells stayed then scraped and sowed into wells at a thickness of 5000 cells per well in poly-L-lysine coated plates. The microtiter plates remained kept on controlled environment of 37 °C, 5% CO_2, and 100% relative humidity for 24 h already added the trial drugs. The trial compounds were added to the cells at a concentration of 50 μg per mL and the plate was then kept on an incubator at 37 °C for 48 h 10 μL of 0.5 mg mL^{-1} of MTT was then added to the solution and then incubated for 3 h at 37 °C and the ending produce formazan crystals stayed measured at 595 nm and 625 nm showed in (Table 5).

3.2.2 MTT-based cytotoxicity activity on lung cancer cell line. In assessing potential for drug toxicity, the name itself suggests that the absence of toxicity alone may not be enough; the presence of other therapeutic properties to anti-mycobacterial activity would need to be established. The concern on toxicity was in the focus regarding the investigated selected structures: two chalcones & five pyrimidine derivatives **4c**, **4g**, **4h**, **4k**, and **4u** on A549 cell lines targeting concentration of 62.5. The information provided indicates that the compounds exhibited moderate toxicity relative to cisplatin. The potent compounds, namely **4g**, showed satisfactory safety profile their IC_{50} showed in (Table 6) against A549 cell line was 49.44 mmol L^{-1} as illustrated in the histogram chart form (Fig. 7).

3.3 Enzyme inhibition studies

As *in vitro* anti-mycobacterial studies, four compounds selected for *in vitro* enzyme inhibition activity against *M. tuberculosis* at a concentration of 50 μM by using the routine method. A triclosan was the first to be tested at the same concentration and 50 mM was able to completely inhibit InhA enzyme. The

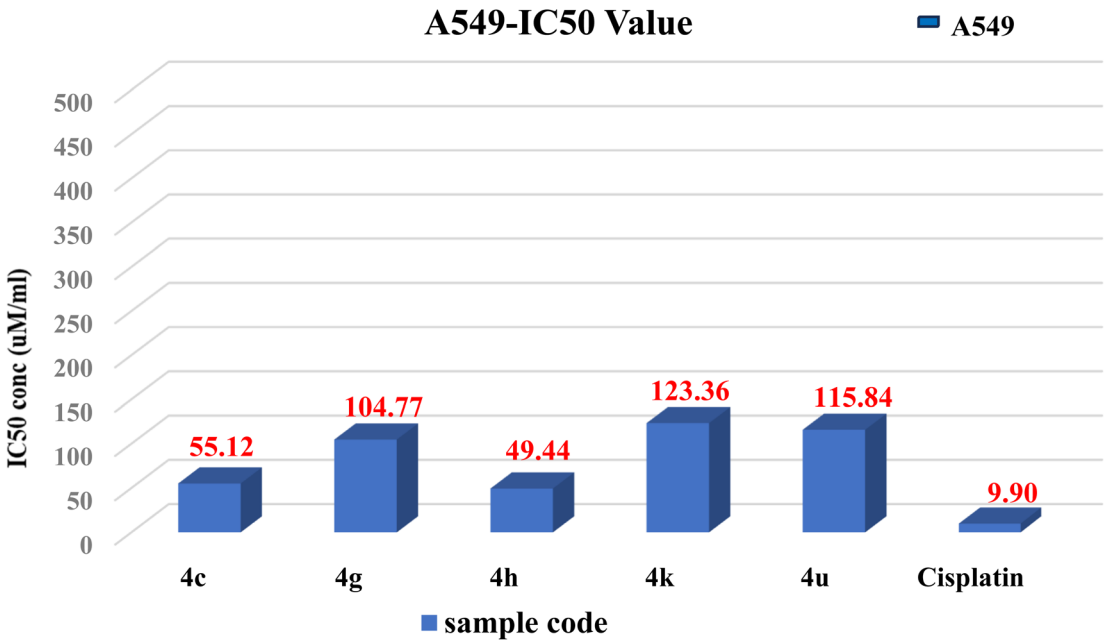

Fig. 7 Overlaid IC_{50} values of given test compounds against A549 cells after the incubation period of 24 h.

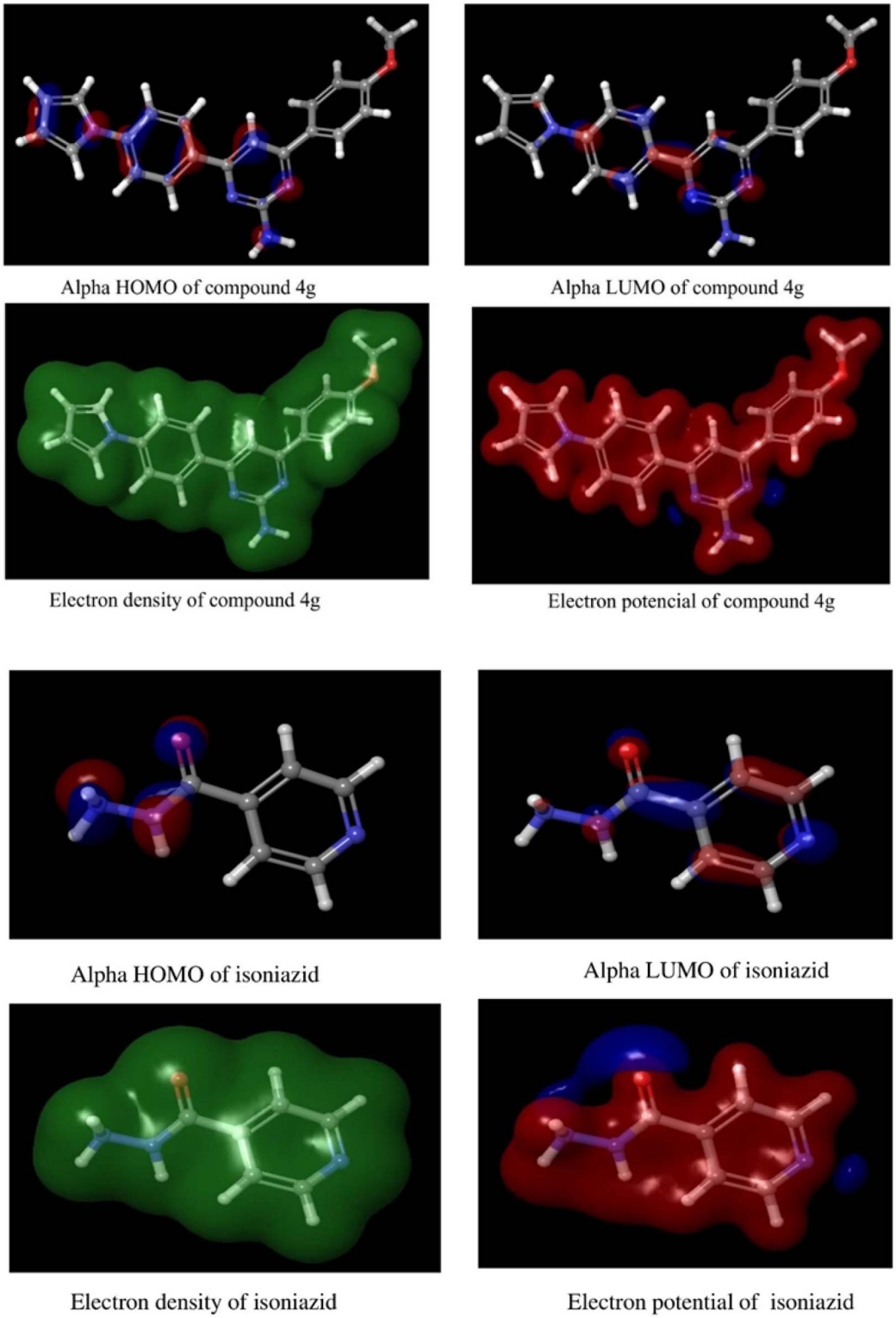

Fig. 8 DFT studies of compound **4g** and standard drug isoniazid.

Table 8 DFT calculation

S. no.	Compound ID	Gas phase energy	Alpha HOMO	Alpha LUMO	Energy gap
1	**4g**	−1105.367894	−0.211939	−0.054720	−0.157219
2	Isoniazid	−472.311674	−0.224326	−0.053617	−0.170716

pyrimidine compounds bearing methoxy group compound **4c**, **4g**, & **4u** on the methoxy aldehyde aromatic group are responsible for inhibition of InhA enzyme. It showed inhibition at 50 μM and 2-thiophene carboxaldehyde substituted and isopropyl group substituted chalcone compound analogue **3k** & **3l**, **4g** showed 36% and **4k** showed 10% inhibition at 50 μM. The outcome shows an increase in the inhibitory action. In antagonist chalcone compound **3k** and **3l**, where thiophene ring at 2nd position substitution with isopropyl group in the 4th position and methoxy group in the pyrimidine ring compounds **3k**, **3l**, **4c**, **4g**, **4h** & **4k** displayed very good % inhibition at 50 μM and **4u** displayed no inhibition, showed in Table 7.

3.4 DFT calculation

Compound **4g** showed total gas phase energy −1105.367894 kcal mol^{-1} and −0.211939 eV and −0.054720 eV for HOMO and LUMO orbitals respectively depicted in (Fig. 8). Overall electron distribution of **4g** was found to be stable. Electrostatic potential was found to be asymmetrically distributed showed. Parallelly, isoniazid as standard drug showed a total gas-phase energy of −0.224326 eV. HOMO and LUMO orbitals of isoniazid showed −0.224326 eV and −0.053617 eV and the energy gap of **4g** compound −0.157219 and isoniazid is −0.170716 depicted in (Table 8). A molecule is considered to be more stable if its energy gap and chemical hardness values are larger. Here **4g** has optimum stability and isoniazid is not showing good stability. The results reveal that of the interplay between molecular geometry and electronic behaviour, shedding light on the chemical properties and potential reactivity of the studied substances. This detailed computational analysis not only contributed to elucidating the structural features but also facilitated the interpretation of the reactivity patterns, enhancing the overall comprehension of the molecular systems being investigated.

3.5 MD simulation

Molecular dynamics simulation predicts the biological system's dynamic nature over a predetermined period of time. MD simulation was carried out in physiological settings to better understand the dynamic nature of the interactions and the stability of the protein–drug complex. Considering the bound free energy values and the XP docking score. Determination of the *in silico* stability of the drug–protein interaction for the docked complex at the molecular level was enhanced by performing MD simulations for 200 ns on all the drug–protein complexes docked (compound **4g** and standard drug isoniazid). Together, these were put through SID (simulation interaction diagram) utility as a 200 ns analysis, which was additionally used by the semi-empirical Desmond module of the Maestro-Schrodinger suite. We analysed the steadiness of the docked compounds within the vigorous pocket of the (5OIR) protein by employing RMSD and its impact on the overall system stability.[48]

3.5.1 RMSD analysis. The root mean square deviation (RMSD) shows the difference between the final positions of the protein backbone (Cα) and the initial structural confirmation. The stability of the protein–ligand complex is measured by the deviation generated during the simulation. These correlations were obtained using InhA instead of the isoniazid PDB: 5OIR model combined with the **4g** compound as the standard for the Multistate modelling. In addition to modelling, all the statistical parameters were put through analysis alongside the generated trajectories of isoniazid, which simultaneously underwent an analysis of RMSD, are illustrated in (Fig. 9) (a) shows the RMSD of the **4g** complex and (b) shows the RMSD of the isoniazid complex. The MD simulation result showed that compound **4g** is stable in a complex with 5OIR. MD simulation of 200 ns in an explicit hydration box was performed to test the stability of **4g**. Comparison of the MD simulation results was performed by evaluation of ligand protein interactions and their contact visualizations, as well as RMSD. In this calculation, the RMSD is used to estimate how much the average of each atom group is displaced relative to a selected atom group across the frames of the trajectory analysis, which is fundamentally aimed at revealing changes in the structure with time. Information on the structural details of a given protein can be obtained by observing the changes of the protein's RMSD during the simulation **4g** ligand & isoniazid RMSD data for certain bound protein and ligand systems.

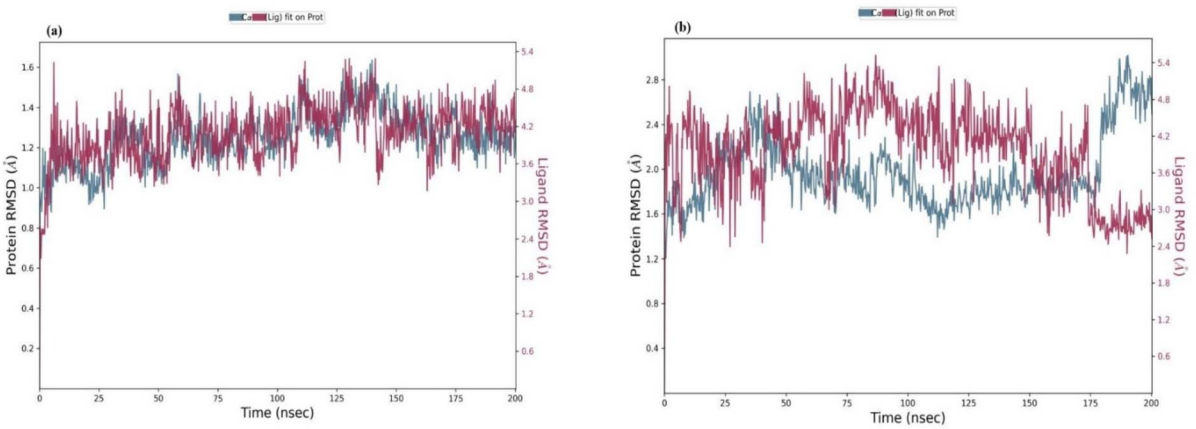

Fig. 9 (a) Shows the RMSD of the **4g** complex and (b) shows the RMSD of the isoniazid complex.

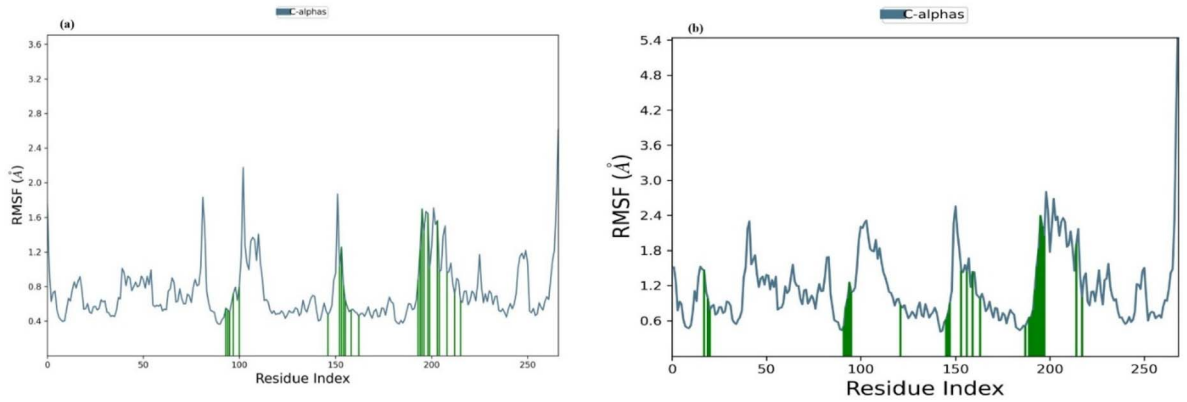

Fig. 10 (a) Shows the RMSF of the **4g** complex and (b) shows the RMSF of the isoniazid complex.

3.5.2 RMSF analysis. The **4g** ligand & isoniazid have specific changes along the peptide bond formation owing to the use of RMSF (Fig. 10) (a) and (b). The interaction of **4g** ligands and the 5OIR protein enzyme occurs during simulation. Each type of interaction has a number of additional more detailed types that can be defined with the help of the 'simulation interactions diagram' panel. Evaluating the RMSF of each amino acid enables an assessment of the stability of the small molecular attached protein compounds. The 5OIR protein attached to compound **4g** and isoniazid displays the RMSF of every amino acid.

Protein–ligand amino acid residue contacts analysis of MD trajectory.

Protein–ligand contact analysis amino acid residues which have positive hydrophobic interactions with the protein with ligands **4g** are Phe 97, Met 103, Phe 149, Met 155, Pro 156, Ala 157, Tyr 158, Met 161, Thr 196, Leu 197, Ala 198, Met 199, Ala 201, Ile 202, Ala 206, Leu 207, Ala 211, Ile 215, and Leu 218. These interactions promote the stabilization of the protein–ligand complex. The water bridges with the ligand that play a significant role in facilitating the interactions among the protein and ligand and a few of the Gly 96, Met 98, Tyr 158, Lys 165, and Leu 197 residues were responsible for the formation of the protein–ligand complex. The hydrogen bonds to the ligand **4g** in (Fig. 11) (a) were in part due to Gly 96 and Gln 100. The residues that facilitated the protein–ligand isoniazid interactions through hydrophobic bonds are: Ser 19, Met 147, Phe 149, Met 161, Val 189, Ala 191. These types of interactions are significant in the maintenance of the protein–ligand complex. The formation of water bridges to the ligand which are of crucial importance to protein–ligand interactions in the form of bridges are constructed by: Ile 21, Ala 22, His 93, Ser 94, Phe 97, Asp 148, Lys 165, Pro 193, Arg 195, Elu 219. The amino His 93, Ser 94, Met155, Lys 165, Ile 194, Thr 196, Leu 197, Ala 198, Met 199 were involved in isoniazid attachment to the protein with the aid of hydrogen bonds in (Fig. 11) (b). The **4g** molecule interacts with 23 amino acids that are present in the 5OIR protein. The residues are constant since the majority of the variations are smaller than 2 Å. For the majority of residues interacting with ligands, the variations are extremely small at 3 nanoseconds. This indicates that the interactions are quite stable during the experiment. During the simulation, the interaction between the ligand and protein was observed. Tyr 158 builds water bridges within the time frame provided, while Gln 100 forms hydrogen bond interaction and Tyr 158 forms hydrophobic interaction for most of the time and water bridges for just a short period of time.

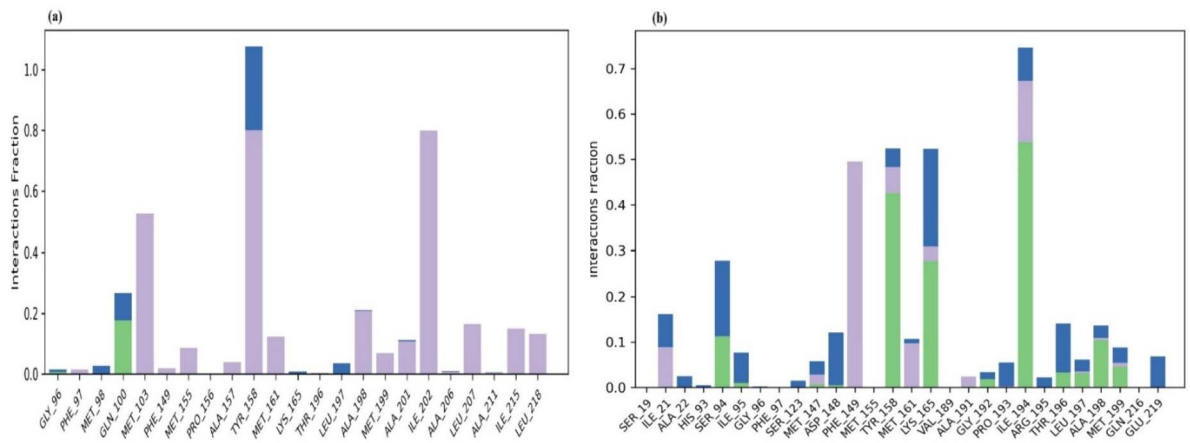

Fig. 11 (a) Protein–ligand amino acid residue contacts of **4g** complex and (b) protein–ligand amino acid residue contacts of isoniazid complex.

3.6 Protein–ligand contact analysis based on the two-dimensional interactions

The precise sequence correlations between the different amino acid residues found in the contact of **4g** with 5OIR protein, **4g** interacts along with the 5OIR protein residues. 51–54% of the simulation period is spent with these interactions steady. Protein–ligand contact analysis based on the two-dimensional interactions which are ligand-mediated is shown. There are also notable Tyr158 and Met103 amino acids that are involved in hydrophobic bonding accounting to some portion of **4g** the compound 46% of the simulation time. Also, for Gln 100, each of 17% polar interactions were noted. For isoniazid protein–ligand contact interaction assessments, the interactions mediated by ligand. The amino acids Phe 149 and Ile 194 have a compound that incorporates 30% of their interaction for 70% of their simulation time.

4. Conclusion

In summary, a series of novel pyrrolyl chalcones and pyrimidine-fused derivatives were successfully synthesized and evaluated for their antitubercular potential. Several compounds, particularly **4g**, demonstrated strong activity against *M. tuberculosis* H37Rv, with minimal cytotoxicity and promising InhA enzyme inhibition. Molecular docking, MM-GBSA, DFT, and MD simulation studies further supported the binding stability and favourable drug-like properties of the active compounds. These findings highlight the potential of these scaffolds as promising leads for the development of new, safe, and effective anti-TB agents targeting InhA.

5. Experimental section

The synthesis was carried out using Sigma-Aldrich® Lab production chemicals & analytical-grade solvents and reagents that were desiccated, purified in accordance with the protocols described in the Vogel's practical book of organic chemistry. To evaluate both the reaction rate and product purity, thin-layer chromatography precoated TLC sheets of silica gel 60 F_{254} (Merck, Darmstadt, Germany) visualized by long- and short-wavelength UV lamps. The mobile phase consisting of *n*-hexane and ethyl acetate in a 6 : 4 ratio. Synthesized compounds were purified *via* recrystallization and column chromatography using by Merck silica gel (70–230 mesh). Melting points were determined using ANALAB scientific melting/boiling point apparatus. FTIR spectra in KBr pellets were recorded on a Bruker FTIR spectrophotometer. The ^{1}H and ^{13}C NMR spectra were recorded using a 400 MHz FT-NMR spectrometer with DMSO-d_6 as the solvent and tetramethyl silane (TMS) as the internal standard, with a sensitivity of δ ppm. The abbreviations used to describe the peak patterns are: (b) broad, (s) singlet, (d) doublet, (t) triplet, (q) quartet, and (m) multiplate. Mass spectra (MS) were recorded in a JEOL GCMATE II GC-mass spectrometer and Shimadzu QP 20105 GC-mass spectrometer.

5.1 General procedure for the synthesis of 1-(4-(1*H*-pyrrol-1-yl)phenyl)-3-substituted prop-2-en-1-ones (3k–3v)

Paal Knorr synthesis was used to constructed pyrrole ring from 4-aminoacetophenone 1 (4.05 g, 0.030 mol) (1) by condensing it with 2,5-dimethoxy tetrahydrofuran (4.23 g, 0.032 mol). Followed by the Claisen Schmidt reaction was used to form chalcones (**3k–3v**) by condensing (2) with different aldehydes using catalytic amount of ethanolic 20 mL NaOH as depicted in Scheme 1. The reaction mixture was stirred for 24–30 h. This was then plunged into cold water and neutralized with hydrochloric acid. The precipitated solid was filtered, washed with water, dried, and purified by column chromatography on silica gel (ethyl acetate/*n*-hexane (6 : 4) then eluent). Compound (**3a–3j**) are used from our earlier reported work[49] and chalcones (**3k–3v**) are reported in this current work.

5.1.1 1-(4-(1*H*-Pyrrol-1-yl)phenyl)-3-(4-isopropylphenyl) prop-2-en-1-one (3k). (Yield 80%). mp 135–137 °C; FTIR (KBr): 1657.65 (C=O) cm^{-1}; ^{1}H NMR (400 MHz, DMSO-d_6) δ ppm: 8.23–8.26 (s, 2H, –CH=CH–), 7.92–8.96 (s, 1H), 7.71–7.84 (m, 5H, bridging phenyl-C_2, C_3, C_5, C_6–H), 7.56–7.57 (s, 2H), 7.33–7.35 (d, J = 8.0 Hz, 2H, pyrrole-C_2, C_4–H), 6.33–6.34 (s, 2H, pyrrole-C_1, C_5–H), 2.92–2.94 (s, 1H), 1.22–1.23 (d, J = 4 Hz, 6H, isopropyl methyl). ^{13}C NMR (100 MHz, DMSO-d_6) δ ppm: 187.68, 151.50, 143.98, 143.21, 134.09, 132.48, 130.53, 129.18, 126.96, 120.95, 119.18, 118.59, 111.56, 33.50, 23.68; MS (ESI): m/z = found 316.15 [M^+ + 1]; calcd. 315.16. Anal. calcd. for $C_{22}H_{21}NO$: C, 83.78; H, 6.71; N, 4.44. Found: C, 83.99; H, 6.80; N, 4.50.

5.1.2 1-(4-(1*H*-Pyrrol-1-yl)phenyl)-3-(thiophen-2-yl)prop-2-en-1-one (3l). (Yield 81%). mp 140–142 °C; FTIR (KBr): 1655.18 (C=O) cm^{-1}; ^{1}H NMR (400 MHz, DMSO-d_6) δ ppm: 8.18–8.20 (d, J = 8 Hz, 2H, –CH=CH–), 7.90–8.94 (s, 1H), 7.71–7.80 (m, 3H) and 7.60–7.64 (d, J = 16 Hz, 1H, bridging phenyl-C_2, C_3, C_5, C_6–H), 7.55–7.56 (s, 1H), 7.52–7.53 (s, 2H, pyrrole-C_2, C_4–H) and 7.19–7.21 (m, 1H, thiophene ring, C_2, C_3, C_4), 6.33–6.34 (s, 2H, pyrrole-C_1, C_5–H). ^{13}C NMR (100 MHz, DMSO-d_6) δ ppm: 187.17, 143.14, 139.75, 136.51, 133.90, 132.77, 130.47, 130.34, 128.71, 120.24, 119.10, 118.59, 111.49; MS(ESI): m/z = found 280.06 [M^+ + 1]; calcd. 279.07. Anal. calcd. for $C_{17}H_{13}NOS$:C, 73.00; H, 4.69; N, 5.05. Found: C, 73.15; H, 4.75; N, 5.19.

5.1.3 1-(4-(1*H*-Pyrrol-1-yl)phenyl)-3-(3,4,5-trimethoxyphenyl)prop-2-en-1-one (3m). (Yield 84%). mp 150–153 °C; FTIR (KBr): 1679.89 (C=O) cm^{-1}; ^{1}H NMR (400 MHz, DMSO-d_6) δ ppm: 8.25–8.27 (d, J = 8.8 Hz, 2H, –CH=CH–), 8.03–8.11 (q, 2H), 7.92–8.01 (s, 1H), 7.80–7.81 (d, J = 4 Hz, 2H), 7.78–7.79 (d, J = 4 Hz, 2H), 7.69–7.74 (m, 2H), 7.51–7.57 (m, 4H, bridging phenyl-C_2, C_3, C_5, C_6–H), 7.23–7.25 (s, 2H, pyrrole-C_2, C_4–H), 6.31–6.35 (m, 2H, pyrrole-C_1, C_5–H), 3.83–3.87 (s, 9H, 3-OCH_3). ^{13}C NMR (100 MHz, DMSO-d_6) δ ppm:153.11, 144.32, 130.49, 119.12, 119.07, 118.55, 111.48, 106.60, 60.13, 56.14; MS(ESI): m/z = found 364.08 [M^+ + 1]; calcd. 363.15. Anal. calcd. for $C_{22}H_{21}NO_4$: C, 72.71; H, 5.82; N, 3.85. Found: C, 72.79; H, 5.90; N, 3.91.

5.1.4 1-(4-(1*H*-Pyrrol-1-yl)phenyl)-3-(4-hydroxy-3,5-dimethoxyphenyl)prop-2-en-1-one (3n). (Yield 80%). mp 141–144 °C; FTIR (KBr): 1677.73 (C=O) cm^{-1}; ^{1}H NMR (400 MHz, DMSO-d_6) δ ppm: 9.055 (s, 1H, –OH), 8.23–8.25 (d, J = 8 Hz, 2H, –CH=CH–), 8.06–8.08 (d, J = 8 Hz, 1H) and 7.67–7.85 (m, 3H,

bridging phenyl-C_2, C_3, C_5, C_6–H), 7.52–7.55 (d, J = 12 Hz, 2H), 7.22 (s, 2H, pyrrole-C_2, C_4–H), 6.34 (s, 2H, pyrrole-C_1, C_5–H), 3.85 (s, 6H, 2-OCH_3); ^{13}C NMR (100 MHz, DMSO-d_6) δ ppm: 198.30, 186.32, 149.21, 143.05, 142.41, 135.30, 133.30, 129.88, 119.06, 118.48, 111.45, 111.25, 55.87; MS(ESI): m/z = found 350.11 [M^+ + 1]; calcd. 349.13. Anal. calcd. for $C_{21}H_{19}NO_4$: C, 72.19; H, 5.48; N, 4.01. Found: C, 72.32; H, 5.50; N, 04.10.

5.1.5 1-(4-(1*H*-Pyrrol-1-yl)phenyl)-3-(4-bromophenyl)prop-2-en-1-one (3o). (Yield 85%). mp 136–138 °C; FTIR (KBr): 1655.31 (C=O) cm^{-1}; ^{1}H NMR (400 MHz, DMSO-d_6) δ ppm: 8.25–8.27 (d, J = 8 Hz, 2H, –CH=CH–), 8.02–8.06 (d, J = 15.6 Hz, 1H), 7.87–7.89 (d, J = 8 Hz, 2H, bromo phenyl C_2, C_4, –H) and 7.78–7.71 (d, J = 9 Hz, 2H, bridging phenyl-C_2, C_3, C_5, C_6–H), 7.70–7.74 (d, J = 15 Hz, 1H) and 7.66–7.68 (d, J = 8 Hz, 1H, bromo phenyl C_1, C_5, –H), 7.56–7.57 (t, 2H, pyrrole-C_1, C_5–H), 6.33–6.34 (t, 2H, pyrrole-C_1, C_5–H). ^{13}C NMR (100 MHz, DMSO-d_6) δ ppm: 143.35, 142.43, 134.04, 131.88, 130.84, 130.58, 123.96, 122.72, 119.14, 118.57, 111.53; MS (ESI): m/z = found 353.11 [M^+ + 2]; calcd. 351.03. Anal. calcd. for $C_{19}H_{14}BrNO$: C, 64.79; H, 4.01; N, 3.08. Found: C, 64.80; H, 4.12; N, 3.12.

5.1.6 1-(4-(1*H*-Pyrrol-1-yl)phenyl)-3-(4-(dimethyl amino) phenyl)prop-2-en-1-one (3p). (Yield 80%). mp 156–159 °C; FTIR (KBr): 1652.7 1 (C=O) cm^{-1}; ^{1}H NMR (400 MHz, DMSO-d_6) δ ppm: 8.19–8.21 (d, J = 8.4 Hz, 2H, –CH=CH–), 7.67–7.77 (m, 6H, bridging phenyl-C_2, C_3, C_5, C_6–H), 7.54–7.55 (t, 2H, pyrrole-C_2, C_4–H), 6.74–6.80 (m, 2H), 6.33–6.33 (t, 2H, pyrrole-C_1, C_5–H), 3.01–3.04 (s, 6H, dimethyl-amino phenyl). ^{13}C NMR (100 MHz, DMSO-d_6) δ ppm: 187.17, 151.99, 145.00, 142.76, 134.80, 130.81, 130.11, 122.04, 119.08, 118.52, 115.90, 111.74, 111.36, 111.06; MS (ESI): m/z = found 317.14 [M^+ + 1]; calcd. 316.16. Anal. calcd. for $C_{21}H_{20}N_2O$: C, 79.72; H, 6.37; N, 8.85. Found: C, 79.80; H, 6.37; N, 8.89.

5.1.7 1-(4-(1*H*-Pyrrol-1-yl)phenyl)-3-(3,4-dimethoxyphenyl) prop-2-en-1-one (3q). (Yield 88%). mp 130–133 °C; FTIR (KBr): 1648.81 (C=O) cm^{-1}; ^{1}H NMR (400 MHz, DMSO-d_6) δ ppm: 8.24–8.26 (d, J = 8 Hz, 2H, –CH=CH–), 7.85–7.89 (d, J = 15 Hz, 1H), 7.77–7.80 (d, J = 8 Hz, 4H, bridging phenyl-C_2, C_3, C_5, C_6–H), 7.70–7.73 (d, J = 15 Hz, 1H), 7.55–7.56 (t, 3H), 7.40–7.42 (dd, J = 10 Hz, 1H) and 7.02–7.04 (d, J = 8.4 Hz, 1H, pyrrole-C_2, C_4–H), 6.33–6.34 (t, 2H, pyrrole-C_1, C_5–H), 3.82–3.87 (s, 6H, 2-OCH_3). ^{13}C NMR (100 MHz, DMSO-d_6) δ ppm: 187.55, 151.29, 149.02, 144.34, 143.04, 134.29, 130.38, 127.55, 123.95, 119.46, 119.11, 118.54, 111.56, 111.44, 110.87, 55.75, 55.60; MS (ESI): m/z = found 334.11 [M^+ + 1]; calcd. 333.14. Anal. calcd. for $C_{21}H_{19}NO_3$: C, 75.66; H, 5.74; N, 4.20. Found: C, 73.70; H, 5.78; N, 4.22.

5.1.8 1-(4-(1*H*-Pyrrol-1-yl)phenyl)-6-phenylhexa-2,5-dien-1-one (3r). (Yield 89%). mp 158–161 °C; FTIR (KBr): 1649.83 (C=O) cm^{-1}; ^{1}H NMR (400 MHz, DMSO-d_6) δ ppm: 8.06–8.08 (d, J = 8 Hz, 2H, –CH=CH–), 7.68–7.77 (m, 2H, pyrrole-C_2, C_4–H), 7.32–7.57 (m, 4H, bridging phenyl-C_2, C_3, C_5, C_6–H), 7.24–7.21 (m, 2H, Ar-phenyl), 7.08–7.10 (m, 3H), 6.27–6.30 (m, 2H, pyrrole-C_1, C_5–H). ^{13}C NMR (100 MHz, DMSO-d_6) δ ppm:144.16, 143.08, 141.61, 130.12, 128.95, 127.30, 127.25, 119.08, 118.6.3, 111.49, 111.44; MS (ESI): m/z = found 314.11 [M^+ + 1]; calcd. 313.15. Anal. calcd. for $C_{22}H_{19}NO$: C, 83.31; H, 6.11; N, 4.47. Found: C, 83.35; H, 6.15; N, 6.15.

5.1.9 1-(4-(1*H*-Pyrrol-1-yl)phenyl)-3-(3-ethoxy-4-hydroxyphenyl)prop-2-en-1-one (3s). (Yield 80%). mp 164–166 °C; FTIR (KBr): 1652.90 (C=O) cm^{-1}; ^{1}H NMR (400 MHz, DMSO-d_6) δ ppm: 8.21–8.23 (d, J = 8 Hz, 2H, –CH=CH–), 7.75–7.77 (d, J = 9 Hz, 2H, CH=CH), 7.64–7.74 (m, 4H, bridging phenyl-C_2, C_3, C_5, C_6–H), 7.54–7.55 (t, 1H), 7.51–7.52 (m, 1H) and 7.46–7.47 (d, J = 4 Hz, 1H, pyrrole-C_2, C_4–H), 7.25–7.27 (d, J = 8 Hz, 1H), 6.77–6.79 (d, J = 8 Hz, 1H), 6.31–6.34 (t, 2H, pyrrole-C_1, C_5–H), 1.35–1.38 (t, 3H, CH_3). ^{13}C NMR (100 MHz, DMSO-d_6) δ ppm:187.31, 147.46, 145.03, 142.86, 134.61, 130.23, 124.62, 119.10, 118.53, 117.47, 115.96, 113.05, 111.38, 63.93; MS(ESI): m/z = found 334.11 [M^+ + 1]; calcd. 333.14. Anal. calcd. for $C_{21}H_{19}NO_3$:C, 75.66; H, 5.74; N, 4.20. Found: C, 75.69; H, 5.76; N, 4.23.

5.1.10 1-(4-(1*H*-Pyrrol-1-yl)phenyl)-3-(3-hydroxy-4-methoxyphenyl)prop-2-en-1-one (3t). (Yield 82%). mp 143–146 °C; FTIR (KBr): 1659.30 (C=O) cm^{-1}; ^{1}H NMR (400 MHz, DMSO-d_6) δ ppm: 9.16 (d, 1H, –OH), 8.21–8.23 (d, J = 8 Hz, 2H, –CH=CH–), 8.01–8.03 (q, 1H), 7.78 (s, 1H), 7.76 (s, 1H) and 7.72–7.74 (d, J = 8 Hz, 2H, bridging phenyl-C_2, C_3, C_5, C_6–H), 7.65 (s, 1H), 7.54–7.56 (m, 2H), 7.29–7.35 (m, 2H, pyrrole-C_2, C_4–H,), 6.91–7.01 (d, 1H) 6.31–6.34 (s, 2H, pyrrole-C_1, C_5–H), 3.36–3.86 (s, 3H, –OCH_3). ^{13}C NMR (100 MHz, DMSO-d_6) δ ppm: 187.54, 150.37.146.78.144.38, 143.02, 134.34, 130.35, 129.89, 127.69, 122.13, 119.25, 119.11, 119.07, 118.57, 118.57, 118.45, 114.93, 111.91, 111.46, 55.69; MS (ESI): m/z = found 320.10 [M^+ + 1]; calcd. 319.12. Anal. calcd. for $C_{20}H_{17}NO_3$: C, 75.22; H, 5.37; N, 4.39. Found: C, 75.28; H, 5.40; N, 4.42.

5.1.11 1-(4-(1*H*-Pyrrol-1-yl)phenyl)-3-(2-hydroxy-3-methoxyphenyl)prop-2-en-1-one (3u). (Yield 89%). mp 151–154 °C; FTIR (KBr): 1641.29 (C=O) cm^{-1}; ^{1}H NMR (400 MHz, DMSO-d_6) δ ppm: 9.16 (d, 1H, –OH), 8.09–8.12 (t, 2H, –CH=CH–), 8.06 (s, 1H, –C=H), 7.84–7.88 (d, J = 15 Hz, 1H), 7.73–7.75 (d, J = 8 Hz, 2H, bridging phenyl-C_2, C_3, C_5, C_6–H), 7.51–7.52 (t, 2H, pyrrole-C_2, C_4–H), 7.21–7.22 (d, J = 7.6 Hz, 1H), 6.74–6.76 (d, J = 7 Hz, 1H) and 6.39 (s, 1H, Ar-phenyl), 6.32–6.33 (t, 2H, pyrrole-C_1, C_5–H), 3.83 (s, 3H 2-OCH_3). ^{13}C NMR (100 MHz, DMSO-d_6) δ ppm: 174.64, 150.37.146.78.144.38, 143.02, 134.34, 130.35, 129.86, 119.06, 118.53, 111.28, 155.69; MS (ESI):m/z = found 320.09 [M^+ + 1]; calcd. 319.12. Anal. calcd. for $C_{22}H_{21}NO$: C, 75.22; H, 5.37; N, 4.39. Found: C, 75.25; H, 5.41; N, 4.43.

5.1.12 1-(4-(1*H*-Pyrrol-1-yl)phenyl)-6-(4-(dimethyl amino) phenyl)hexa-2,5-dien-1-one (3v). (Yield 85%). mp 162–165 °C; FTIR (KBr): 1641.91 (C=O) cm^{-1}; ^{1}H NMR (400 MHz, DMSO-d_6) δ ppm: 8.09–8.010 (q, 4H, –CH=CH–), 7.73–7.78 (t, 4H, bridging phenyl-C_2, C_3, C_5, C_6–H), 7.43–7.54 (q, 4H, pyrrole-C_2, C_4–H and Ar-phenyl), 6.32–6.33 (t, 4H, pyrrole-C_1, C_5–H and CH=CH), 2.58–2.97 (s, 6H, –$2CH_3$). ^{13}C NMR (100 MHz, DMSO-d_6) δ ppm: 196.65, 143.15, 133.33, 130.07, 129.90, 128.88, 119.07, 118.60, 118.44, 112.00, 111.45, 26.60; MS (ESI): m/z = found 357.15 [M^+ + 1]; calcd. 356.19. Anal. calcd. for $C_{24}H_{24}N_2O$: C, 80.87; H, 6.79; N, 7.86. Found: C, 80.92; H, 6.83; N, 7.88.

5.2 General procedure to synthesis of 4-(4-(1*H*-pyrrol-1-yl) phenyl)-6-phenylpyrimidin-2-amine (4a–4v)

Chalcones (**3a–3v**) were cyclized to pyrimidine by reacting with Guanidine hydrochloride (0.007 mol) in the presence of sodium

ethoxide (0.02 mol) and dried DMF (15 mL) as a solvent as depicted in scheme −2. Reaction mixture was refluxed at 80 °C for 30–35 h, and reaction progress monitored by TLC. The reaction was quenched with crushed ice, yielding a ppt solid which was filtered off, washed with water, hydrated and purified by column-chromatography (2 : 1), ethyl acetate and *n*-hexan.

5.2.1 4-(4-(1*H*-Pyrrol-1-yl)phenyl)-6-(4-chlorophenyl) pyrimidin-2-amine (4a). (Yield 88%). mp 142–144 °C; FTIR (KBr): 3486.01, 3194.81 cm^{-1} (–NH_2), 1596.79 cm^{-1} (Ar C=C). ^{1}H NMR (400 MHz, DMSO-d_6) δ 8.29–8.31 (d, J = 8 Hz, 1H), 8.24–8.26 (d, J = 8 Hz, 2H) and 7.92 (s, 2H, bridging phenyl-C_2, C_3, C_5, C_6–H), 7.73–7.76(d, J = 12, 2H, Ar-phenyl), 7.58–7.71 (t, 2H, Ar-phenyl), 7.56 (s, 2H, pyrrole-C_2, C_4–H), 7.49 (s, 2H, –NH_2), 6.29–6.76 (s, 2H, pyrrole-C_1, C_5–H); ^{13}C NMR (100 MHz, DMSO-d_6) δ 16, 4.02, 164.41, 164.41, 164.62, 141.92, 136.66, 135.68, 134.20, 129.27, 129.12, 129.27, 128.94, 119.46, 119.32, 111.43, 101.88. MS (ESI): m/z = found (M^+ + 1) 347.19, calc 346.10. Anal. calcd. for $C_{20}H_{15}ClN_4$: C, 69.26; H, 4.36; N, 16.15. Found: C, 69.30; H, 4.40; N, 16.20.

5.2.2 4-(4-(1*H*-Pyrrol-1-yl)phenyl)-6-(furan-3-yl)pyrimidin-2-amine (4b). (Yield 82%). mp 168–169 °C; FTIR (KBr): 3468.18, 3158.90 cm^{-1} (NH_2), 1569.81 cm^{-1} (Ar C=C). ^{1}H NMR (400 MHz, DMSO-d_6) δ 8.14–8.16 (d, J = 8 Hz, 2H), and 7.44–7.61 (s, 2H, bridging phenyl-C_2, C_3, C_5, C_6–H), 7.27 (s, 2H, pyrrole-C_2, C_4–H), 7.21–7.22 (d, J = 3, 1H), 7.18–7.19 (d, J = 4 Hz, 3H, –furfural ring), 6.58–6.59 (q, 1H, –CH=CH, pyrimidine ring), 6.39–6.40 (t, J = 4 Hz, 2H, pyrrole-C_1, C_5–H), 5.22 (s, 2H, –NH_2). ^{13}C NMR (100 MHz, DMSO-d_6) δ 164.75, 164.39, 163.57, 141.96, 140.15, 133.55, 134.14, 131.2, 130.00, 129.02, 128.86, 127.09, 127.54, 119.33, 119.45, 111. 40, 24.2. MS (ESI): m/z = found (M^+ + 1) 303.12, calc. 302.12. Anal. calcd. For $C_{18}H_{14}N_4$: C, 71.51; H, 4.67; N, 18.53. Found: C, 71.56; H, 4.40; N, 18.58.

5.2.3 4-(4-(1*H*-Pyrrol-1-yl)phenyl)-6-(2,4-dimethoxyphenyl) pyrimidin-2-amine (4c). (Yield 88%). mp 160–162 °C; FTIR (KBr): 3374.53, 2935.68 cm^{-1} (NH_2), cm^{-1} (Ar–C=O), 1563.58 cm^{-1} (Ar C=C). ^{1}H NMR (400 MHz, DMSO-d_6) δ 8.12–8.14 (d, J = 8.4 Hz, 1H, CH=CH), 7.87–7.89 (d, J = 8 Hz, 1H), and 7.34–7.75 (m, 2H,) and 6.68–6.70 (s, 1H, bridging phenyl-C_2, C_3, C_5, C_6–H), 6.61–6.67 (d, J = 2 Hz, 2H, pyrrole-C_2, C_4–H), 6.48–6.56 (s, 3H, Ar-phenyl), 6.31–6.32 (s, 2H, pyrrole-C_1, C_5–H), 6.25–6.26 (d, J = 4 Hz, 2H, –NH_2), 3.84–3.90 (s, 3H–OCH_3), 3.41–3.51 (s, 3H, –OCH_3). ^{13}C NMR (100 MHz, DMSO-d_6) δ 164.20, 163.11, 162.46, 159.59, 141.65, 134.68, 131.85, 130.58, 128.60, 128.39, 126.65, 119.71, 119.53, 119.38, 119.24, 118.99, 111.96, 111.44, 110.83, 106.01, 99.14, 56.26–55.69; MS (ESI): m/z = found (M^+ + 1) 373.15, calc. 372.16. Anal. calcd. For $C_{22}H_{20}N_4O_2$: C, 70.95; H, 5.41; N, 15.04. Found: C, 70.98; H, 5.45; N, 15.09.

5.2.4 4-(4-(1*H*-Pyrrol-1-yl)phenyl)-6-phenylpyrimidin-2-amine (4d). (Yield 84%). mp 149–150 °C; FTIR (KBr): 3300.12, 3189.44 cm^{-1} (NH_2), cm^{-1} (Ar–C=O), 1565.41 cm^{-1} (Ar C=C). ^{1}H NMR (400 MHz, DMSO-d_6) δ 8.31–8.29 (d, J = 8 Hz, 1H, Ar phenyl) and 8.26–8.24 (d, J = 8 Hz, 1H, –CH=CH pyrimidine ring), 7.92 (s, 2H, bridging phenyl-C_2, C_6–H), 7.73–7.71 (t, 2H, bridging phenyl- C_3, C_5, –H), 7.58–7.56 (d, J = 8.4 Hz, 3H, Ar phenyl), 7.49 (s, 2H, pyrrole-C_2, C_4–H) 6.76 (s, 2H, NH_2), 6.29 (s, 2H, pyrrole-C_1, C_5–H). ^{13}C NMR (100 MHz, DMSO-d_6) δ 165.33, 164.45, 164.38, 141.85, 137.85, 134.34, 130.91, 129.07, 128.90, 127.48, 119.45, 119.33, 111.93, 111.42, 101.97. MS (ESI): m/z = found (M^+ + 1) 313.16, calc. 312.14. Anal. calcd. for $C_{20}H_{16}N_4$: C, 76.90; H, 5.16; N, 17.94. Found: C, 76.91; H, 5.18; N, 17.97.

5.2.5 4-(4-(1*H*-Pyrrol-1-yl)phenyl)-6-(*p*-tolyl)pyrimidin-2-amine (4e). (Yield 85%). mp 160–161 °C; FTIR (KBr): 3495.20, 3303.21 cm^{-1} (NH_2), cm^{-1} (Ar–C=O), 1575.64 cm^{-1} (Ar C=C). ^{1}H NMR (400 MHz, $CDCl_3$) δ 8.13–8.15 (d, J = 8.4 Hz, 2H, –CH=CH, pyrimidine ring), 7.97–7.99 (d, J = 8 Hz, 2H bridging phenyl-C_2, C_6–H), 7.51–7.53 (d, J = 8 Hz, 2H, bridging phenyl-C_3, C_5, –H), 7.45 (s, 1H, Ar phenyl), 7.31–7.33 (d, J = 8 Hz, 2H), 7.12 (s, 1H, Ar phenyl), 7.10–7.12 (d, J = 6.4 Hz, 2H, pyrrole-C_2, C_4–H), 7.063 (s, 1H, –CH=CH pyrimidine ring) 6.34–6.41 (s, 2H, pyrrole-C_1, C_5–H), 5.35 (s, 2H, –NH_2), 2.26–2.45 (s, 3H, –CH_3). ^{13}C NMR (100 MHz, DMSO-d_6) δ 165.23, 164.40, 164.24, 141.81, 140.72, 130.82, 129.86, 129.67, 128.87, 127.40. MS (ESI): m/z = found (M^+ + 1) 327.15, calc. 326.15. Anal. calcd. for $C_{21}H_{18}N_4$: C, 77.28; H, 5.56; N, 17.17. Found: C, 77.31; H, 5.59; N, 17.20.

5.2.6 4-(4-(1*H*-Pyrrol-1-yl)phenyl)-6-(3-bromophenyl) pyrimidin-2-amine (4f). (Yield 89%). mp 157–158 °C; FTIR (KBr): 3482.21, 3304.86 cm^{-1} (NH_2), cm^{-1} (Ar–C=O), 1562.43 cm^{-1} (Ar C=C). ^{1}H NMR (400 MHz, $CDCl_3$) δ 8.23 (s, 1H, –CH=CH, pyrimidine ring), 8.12–8.15 (d, J = 8.8 Hz, 2H, bridging phenyl-C_2, C_6–H), 7.96–7.98 (d, J = 8 Hz 2H, bridging phenyl-C_3, C_5, –H), 7.60–7.62 (d, J = 7 Hz 1H, Ar phenyl), 7.50–7.52 (d, J = 8, 2H, pyrrole-C_2, C_4–H), 7.34–7.42 (q, 3H, Ar phenyl), 7.25 (s, 2H), 6.39 (s, 2H, pyrrole-C_1, C_5–H), 5.23 (s, 2H, –NH_2). ^{13}C NMR (100 MHz, DMSO-d_6) δ164.75, 164.39, 163.57, 141.46, 140.15, 134.14, 133.55, 131.25, 130.00, 129.02, 126.48, 122.69, 119.54, 119.46, 119.30, 118.92, 111.93, 111.44, 102.08. MS (ESI): m/z = found (M^+ + 2)393.04, calc. 390.05. Anal. calcd. For $C_{20}H_{15}BrN_4$: C, 61.39; H, 3.86; N, 14.32. Found: C, 61.41; H, 3.89; N, 14.36.

5.2.7 4-(4-(1*H*-Pyrrol-1-yl)phenyl)-6-(4-methoxyphenyl) pyrimidin-2-amine (4g). (Yield 85%). mp 168–169 °C; FTIR (KBr): 3498.80, 3382.39 cm^{-1} (NH_2), cm^{-1} (Ar–C=O), 1537.69 cm^{-1} (Ar C=C). ^{1}H NMR (400 MHz, $CDCl_3$) δ 8.13–8.15 (d, J = 8.8 Hz, 2H) and 8.05–8.07 (d, J = 8.8 Hz, 2H, bridging phenyl-C_2, C_3, C_5, C_6–H), 7.50–7.52 (d, J = 8.4 Hz 2H, Ar phenyl), 7.42 (s, 1H CH=CH pyrimidine ring), 7.18–7.27 (s, 2H, pyrrole-C_2, C_4–H), 7.01–7.03 (d, J = 8.0 Hz, 2H, Ar phenyl), 6.40 (s, 2H, pyrrole-C_1, C_5–H), 5.25 (s, 2H, –NH_2), 3.70–3.89 (t, 3H, –OCH_3). ^{13}C NMR (100 MHz, DMSO-d_6) δ 164.89, 164.34, 164.07, 161.71, 141.76, 134.49, 130.11, 129.06, 128.85, 119.44, 119.32, 114.41, 111.40, 101.20, 55.79. MS (ESI): m/z = found (M^+ + 1) 343.14, calc. 342.40. Anal. calcd. for $C_{21}H_{18}N_4O$: C, 75.67; H, 5.30; N, 16.36. Found: C, 75.70; H, 5.32; N, 16.38.

5.2.8 4-(4-(1*H*-Pyrrol-1-yl)phenyl)-6-(2,4-dichlorophenyl) pyrimidin-2-amine (4h). (Yield 80%). mp 144–145 °C; FTIR (KBr): 3308.41 cm^{-1} (NH_2), cm^{-1} (Ar–C=O), 1589.71 cm^{-1} (Ar C=C). ^{1}H NMR (400 MHz, DMSO-d_6) δ 8.09–8.11 (d, J = 8 Hz, 2H) and 7.57–759 (d, 2H, bridging phenyl-C_2, C_3, C_5, C_6–H), 7.48–7.50 (d, 2H), 7.17–7.25 (s, 2H pyrrole-C_2, C_4–H), 7.16–7.17 (t, 2H, -Ar phenyl), 6.32–6.38 (s, 2H, pyrrole-C_1, C_5–H), 2.86–2.95 (s, 2H, NH_2). ^{13}C NMR (100 MHz, DMSO-d_6) δ 163.32, 162.02, 140.82, 135.00, 130.16, 129.30, 128.55, 124.36, 119.36, 119.21, 110.53, 101.83. MS (ESI): m/z = found (M^+ + 1) 381.03, calc.

380.06. Anal. calcd. for $C_{20}H_{14}Cl_2N_4$: C, 63.01; H, 3.70; N, 14.70. Found: C, 63.03; H, 3.73; N, 14.76.

5.2.9 2-(6-(4-(1*H*-Pyrrol-1-yl)phenyl)-2-aminopyrimidin-4-yl)phenol (4i). (Yield 88%). mp 157–158 °C; FTIR (KBr): 3359.43 cm^{-1} (NH_2), cm^{-1} (Ar–C=O), 1577.36 cm^{-1} (Ar C=C). ^1H NMR (400 MHz, DMSO-d_6) δ 8.11–8.13 (d, J = 8 Hz, 1H, –CH=CH, Ar phenyl), 8.01–8.03 (d, 2H, J = 8 Hz, 1H, –CH=CH, pyrimidine ring), 7.86–7.88 (d, J = 8 Hz, H, Ar phenyl), 7.43–7.55 (m, 4H, bridging phenyl-C_2, C_3, C_5, C_6–H), 7.35–7.39 (m, 2H pyrrole-C_2, C_4–H), 7.25 (s, 1H, –OH), 7.17–7.18 (t, 3H, Ar phenyl), 7.03–6.92 (m, 2H, pyrrole-C_1, C_5–H), 6.39 (s, 2H, NH_2). ^{13}C NMR (100 MHz, DMSO-d_6) δ 164.70, 164.67, 163.40, 141.76, 140.25, 134.10, 133.44, 131.20, 130.00, 129.01, 126.39, 122.48, 119.55, 119.43, 119.29, 118.90, 111.83, 111.84, 102.09. MS (ESI): m/z = found (M^+ + 1) 329.11, calc. 328.13. Anal. calcd. for $C_{20}H_{16}N_4O$: C, 73.15; H, 4.91; N, 17.06. Found: C, 73.18; H, 4.94; N, 17.09.

5.2.10 4-(4-(1*H*-Pyrrol-1-yl)phenyl)-6-(2,6-dichlorophenyl) pyrimidin-2-amine (4j). (Yield 82%). mp 147–148 °C; FTIR (KBr): 3290.74, 3146.69 cm^{-1} (NH_2), cm^{-1} (Ar–C=O), 1569.58 cm^{-1} (Ar C=C). ^1H NMR (400 MHz, DMSO-d_6) δ 8.03–8.10 (, 2H, *d*, J = 8 Hz, 1H, –CH=CH, pyrimidine ring), 7.59–7.507 (d, J = 8 Hz, 1H, –CH=CH, Ar phenyl), 7.48–7.50 (d, J = 8 Hz, 2H bridging phenyl-C_3, C_5, –H), 7.37–7.36,(d, J = 8 Hz, 2H, bridging phenyl-C_2, C_6), 7.25 (s, 1H, –CH=CH, Ar phenyl), 7.08–7.09, (s 2H, pyrrole-C_2, C_4–H), 6.38 (s, 2H, pyrrole-C_1, C_5–H), 5.24–5.28 (s, 2H, NH_2). ^{13}C NMR (100 MHz, DMSO-d_6) δ164.82, 164.69, 141.43, 137.30, 134.50, 132.30, 129.52, 128.65, 124.76, 119.50, 119.30, 111.03, 110.33. MS (ESI): m/z = found (M^+ + 1) 381.02, calc. 380.06. Anal. calcd. for $C_{20}H_{14}Cl_2N_4$: C, 63.01; H, 3.70; N, 14.70. Found: C, 63.05; H, 3.72; N, 14.73.

5.2.11 4-(4-(1*H*-Pyrrol-1-yl)phenyl)-6-(4-isopropylphenyl) pyrimidin-2-amine (4k). (Yield 90%). mp 169–170 °C; FTIR (KBr): 3320.38, 2958.59 cm^{-1} (NH_2), 1516.23 cm^{-1} (Ar C=C). ^1H NMR (400 MHz, DMSO-d_6) δ 8.31–8.33 (d, J = 8 Hz, 2H, Ar phenyl) and 8.18–8.61 (d, J = 7 Hz, 2H, bridging phenyl-C_2, C_3, C_5, C_6–H), 7.72–7.75 (t, 4H Ar phenyl), 7.54 (s, 1H, –CH=CH pyrimidine ring), 7.51 (s, 1H, –CH=CH), 7.38–7.40 (d, J = 8 Hz, 2H), 7.25–7.27 (d, J = 9 Hz, 2H, pyrrole-C_2, C_4–H), 6.26 (s, 2H, pyrrole-C_1, C_5–H), 6.70 (s, 2H, NH_2), 1.07–1.26 (m, 6H, isopropyl 2-CH_3). ^{13}C NMR (100 MHz, DMSO-d_6) δ 164.14, 164.29, 157.00, 152.51, 145.72, 141.91, 119.39, 112.90, 112.14, 111.45, 99.9. MS (ESI): m/z = found (M^+ + 1) 355.17, calc. 354.18. Anal. calcd. for $C_{23}H_{22}N_4$: C, 77.94; H, 6.26; N, 15.81. Found: C, 77.96; H, 6.28; N, 15.83.

5.2.12 4-(4-(1*H*-Pyrrol-1-yl)phenyl)-6-(thiophen-2-yl) pyrimidin-2-amine (4l). (Yield 89%). mp 155–156 °C; FTIR (KBr): 3290.74, 3146.69 cm^{-1} (NH_2), 1569.58 cm^{-1} (Ar C=C). ^1H NMR (400 MHz, DMSO-d_6) δ 8.29–8.31 (d, J = 8 Hz, 2H, –CH=CH, pyrimidine ring), 8.159–8.151 (d, J = 3 Hz, 2H, –CH=CH, thiophene ring), 7.74–7.78 (s, 4H, bridging phenyl-C_2, C_3, C_5, C_6–H), 7.51–7.52 (s, 2H, pyrrole-C_2, C_4–H), 7.23–7.25 (d, J = 8 Hz 1H, –CH=CH, thiophene ring), 6.32 (s, 2H, pyrrole-C_1, C_5–H), 6.76 (s, 2H, NH_2). ^{13}C NMR (100 MHz, DMSO-d_6) δ164.13, 164.00, 160.54, 143.76, 141.89, 134.10, 130.30, 128.87, 128.82, 128.45, 119.31, 111.43, 100.30. MS(ESI): m/z = found (M^+ + 1) 319.07, calc. 318.09. Anal. calcd. for $C_{18}H_{14}N_4S$: C, 67.90; H, 4.43; N, 17.06. Found: C, 67.92; H, 4.44; N, 17.08.

5.2.13 4-(4-(1*H*-Pyrrol-1-yl)phenyl)-6-(3,4,5-trimethoxyphenyl)pyrimidin-2-amine (4m). (Yield 89%). mp 170–171 °C; FTIR (KBr): 3376.01, 2937.70 cm^1(NH_2), 1596.38 cm^{-1} (Ar C=C). ^1H NMR (400 MHz, DMSO-d_6) δ 8.33–8.35 (d, J = 8 Hz, 2H, Ar phenyl), 7.46–7.74 (t, 4H, bridging phenyl-C_2, C_3, C_5, C_6–H), 7.50–7.53 (q, 2H, pyrrole-C_2, C_4–H, 1H, –CH=CH pyrimidine ring), 6.74 (s, 2H, pyrrole-C_1, C_5–H), 6.33 (s, 2H, NH_2), 3.75–3.92 (s, 6H, 2OCH_3), 3.35 (s, 3H, OCH_3). ^{13}C NMR (100 MHz, DMSO-d_6) δ 164.28, 153.49, 128.8, 119.47, 119.31, 111.42, 104.98, 60.61, 56.61. MS (ESI): m/z = found (M^+ + 1) 403.16, calc. 402.17. Anal. calcd. for $C_{23}H_{22}N_4O_3$: C, 68.64; H, 5.51; N, 13.92. Found: C, 68.66; H, 5.53; N, 13.94.

5.2.14 4-(6-(4-(1*H*-Pyrrol-1-yl)phenyl)-2-aminopyrimidin-4-yl)-2,6-dimethoxyphenol (4n). (Yield 80%). mp 154–155 °C; FTIR (KBr): 3367.29 cm^{-1} (NH_2), (Ar–C=O), 1569.38 cm^{-1} (Ar C=C). ^1H NMR (400 MHz, DMSO-d_6) δ 8.11–8.13 (d, J = 8 Hz, 2H, Ar phenyl), 8.08–8.10 (t, OH), 7.46–7.52 (m, 4H, bridging phenyl-C_2, C_3, C_5, C_6–H), 7.34–7.37 (J = 8 Hz, 2H, pyrrole-C_2, C_4–H), 7.25 (s, H, –CH=CH pyrimidine ring), 7.16–7.17 (s, 2H, pyrrole-C_1, C_5–H), 6.38–6.39 (s, 3H, Ar phenyl), 5.16 (s, 2H, NH_2), 4.00 (s, 3H, OCH_3). ^{13}C NMR (100 MHz, DMSO-d_6) δ165.24, 164.22, 148.44, 143.62, 141.75, 138.81, 134.58, 130.36, 128.91, 127.87, 119.55, 119.45, 119.40, 119.29, 118.97, 118.91, 111.94, 111.39, 105.26, 56.71, 27.10. MS (ESI): m/z = found (M^+ + 1) 389.11, calc. 388.15. Anal. calcd. for $C_{22}H_{20}N_4O_3$: C, 68.03; H, 5.19; N, 14.42. Found: C, 68.05; H, 5.21; N, 14.45.

5.2.15 4-(4-(1*H*-Pyrrol-1-yl)phenyl)-6-(4-bromophenyl) pyrimidin-2-amine (4o). (Yield 85%). mp 161–162 °C; FTIR (KBr): 3465.31 cm^{-1} (NH_2), cm^{-1} (Ar–C=O), 1564.81 cm^{-1} (Ar C=C). ^1H NMR (400 MHz, DMSO-d_6) δ 8.11–8.13 (d, J = 8 Hz, 2H, Ar-phenyl), 7.93–7.95 (d, J = 8 Hz, 2H, bridging phenyl-C_2, C_6–H), 7.61–7.63 (d, J = 8 Hz, 2H, bridging phenyl-C_3, C_5–H), 7.49–7.51 (d, J = 8 Hz, 2H, pyrrole-C_2, C_4–H), 7.41 (s, 1H, CH=CH, pyrimidine ring), 7.16–7.24 (s, 2H, Ar phenyl), 6.38 (s, 2H, pyrrole- C_1, C_5–H), 5.24 (s, 2H, NH_2). ^{13}C NMR (100 MHz, DMSO-d_6) δ 164.42, 164.09, 141.92, 137.02, 134.19, 132.06, 129.52, 128.95, 124.56, 119.46, 119.31, 111.43, 101.83. MS (ESI): m/z = found (M^+ + 1) 391.91, calc. 390.05. Anal. calcd. for $C_{20}H_{15}BrN_4$: C, 61.39; H, 3.86; N, 14.32. Found: C, 61.43; H, 3.87; N, 14.34.

5.2.16 4-(4-(1*H*-Pyrrol-1-yl)phenyl)-6-(4-(dimethyl amino) phenyl)pyrimidin-2-amine (4p). (Yield 87%). mp 156–157 °C; FTIR (KBr): 3309.53, 3192.65, 2913.18 cm^{-1} (NH_2), cm^{-1} (Ar–C=O), 1561.02 cm^{-1} (Ar C=C). ^1H NMR (400 MHz, DMSO-d_6) δ 8.02–8.12 (d, J = 8 Hz, 2H, Ar phenyl), 7.48–7.50 (d, 2H, pyrrole-C_2, C_4–H, and 1H, –CH=CH, pyrimidine ring), 7.39-(s, 2H, bridging phenyl-C_2, C_3, C_5, C_6–H), 7.17 (s, 2H, Ar phenyl), and 6.76–6.78 (d, 2H, Ar phenyl), and 6.38 (s, 2H, NH_2), 5.22 (s, 2H, pyrrole-C_1, C_5–H), 3.04 (s, 6H, 2CH_3); ^{13}C NMR (100 MHz, DMSO-d_6) δ 166.02, 164.29, 163.54, 152.12, 141.97, 135.23, 128.38, 128.70, 128.27, 124.69, 120.05, 119.13, 111.75, 110.90, 102.40, 77.35, 77.03, 76.72. MS (ESI): m/z = found (M^+ + 1) 356.91, calc. 355.00. Anal. calcd. for $C_{22}H_{21}N_5$: C, 74.34; H, 5.96; N, 19.70. Found: C, 74.36; H, 5.99; N, 19.72.

5.2.17 4-(4-(1*H*-Pyrrol-1-yl)phenyl)-6-(3,4-dimethoxyphenyl) pyrimidin-2-amine (4q). (Yield 89%). mp 174–175 °C; FTIR (KBr): 3518.91, 2934.70 cm^{-1} (NH_2), cm^{-1} (Ar–C=O),

1596.79 cm^{-1} (Ar C=C). ^1H NMR (400 MHz, DMSO-d_6) δ 8.18–8.20 (d, J = 8 Hz, 2H, Ar phenyl), 7.78 (s, 1H, –CH=CH, pyrimidine ring), 7.69–7.71 (d, 1H, Ar phenyl), 7.55–7.57 (d, 2H, pyrrole-C_2, C_4–H), 7.01–7.47 (m, 4H, bridging phenyl-C_2, C_3, C_5, C_6–H), 6.45 (s, 2H), 7.07–7.17 (s, 2H), 6.262–6.32 (s, 2H, pyrrole-C_1, C_5–H).5.39 (s, 2H, NH_2), 4.01–4.07 (s, 6H, 2-OCH_3). ^{13}C NMR (100 MHz, DMSO-d_6) δ 165.72, 164.83, 163.52, 151.27, 149.23, 134.77, 130.29, 128.47, 120.17, 120.05, 119.10, 111.03, 110.90, 109.97, 103.18, 77.37, 77.04, 76.73, 56.04, 56.00. MS (ESI): m/z = found (M^++) 372.91, calc. 372.16. Anal. calcd. for $C_{22}H_{20}N_4O_2$: C, 70.95; H, 5.41; N, 15.04. Found: C, 70.97; H, 5.42; N, 15.06.

5.2.18 4-(4-(1*H*-Pyrrol-1-yl)phenyl)-6-styrylpyrimidin-2-amine (4r). (Yield 86%). mp 154–155 °C; FTIR (KBr): 3325.08, 3185.10 cm^{-1} (NH_2), cm^{-1} (Ar–C=O), 1564.46 cm^{-1} (Ar C=C). ^1H NMR (400 MHz, DMSO-d_6) δ 8.11–8.14 (d, J = 8 Hz, 2H, Ar phenyl), 7.86 (s, 1H, –CH=CH, pyrimidine ring), 7.82 (s, 2H, pyrrole-C_2, C_4–H), 7.61–7.63 (d, J = 7 Hz, 3H, Ar phenyl), 7.12–7.50 (m, 4H, bridging phenyl-C_2, C_3, C_5, C_6–H), 7.01–7.05 (s, 2H, –CH=CH, aliphatic chain), 6.40–6.41 (s, 2H, pyrrole- C_1, C_5–H), 5.17 (s, 2H, NH_2). ^{13}C NMR (100 MHz, DMSO-d_6) δ 164.96, 164.11, 163.35, 142.27, 136.14, 135.94, 134.50, 129.12, 128.43, 127.56, 126.49, 120.06, 119.10, 111.03, 105.81. MS (ESI): m/z = found (M^++) 338.90, calc. 338.15. Anal. calcd. for $C_{22}H_{18}N_4$: C, 78.06; H, 5.36; N, 16.56. Found: C, 78.08; H, 5.39; N, 16.59.

5.2.19 4-(6-(4-(1*H*-Pyrrol-1-yl)phenyl)-2-aminopyrimidin-4-yl)-2-ethoxyphenol (4s). (Yield 87%). mp 194–196 °C; FTIR (KBr): 3510.82, 3394.67, cm^{-1} (NH_2), cm^{-1} (Ar–C=O), 1566.53 cm^{-1} (Ar C=C). ^1H NMR (400 MHz, DMSO-d_6) δ 9.45 (s, 1H, OH), 8.30–8.32 (d, 2H, –CH, Ar), 7.49–7.80 (m, 7H, bridging phenyl-C_2, C_3, C_5, C_6–H and -Ar), 7.82 (s, 2H, pyrrole-C_1, C_5–H), 6.91–6.93 (d, J = 8.0 Hz, 1H), 6.62 (s, 2H, pyrrole-C_2, C_4–H), 6.31 (s, 2H, NH_2), 4.14–4.16 (s, 2H, –CH), 3.36 (s, 1H, –CH), 1.37–1.41 (s, 3H–CH); ^{13}C NMR (100 MHz, DMSO-d_6) δ 165.21, 164.26, 149.96, 147.28, 141.68, 134.58, 129.00, 128.82, 121.10, 119.41, 119.29, 115.93, 112.71, 111.36, 101.15, 64.61, 15.28. MS (ESI): m/z = found (M^+ + 1) 372.91, calc. 372.16. Mass calc 372.16, Found (M^++)372.91. Anal. calcd. for $C_{22}H_{20}N_4O_2$: C, 70.95; H, 5.41; N, 15.04. Found: C, 70.99; H, 5.43; N, 15.06.

5.2.20 5-(6-(4-(1*H*-Pyrrol-1-yl)phenyl)-2-aminopyrimidin-4-yl)-2-methoxyphenol (4t). (Yield 82%). mp 189–190 °C; FTIR (KBr): 3340.91 cm^{-1} (NH_2), cm^{-1} (Ar–C=O), 1568.87 cm^{-1} (Ar C=C). ^1H NMR (400 MHz, DMSO-d_6) δ 8.27–8.29 (s, 1H, OH), 8.03–8.14 (d, J = 8.0 Hz, 1H, Ar-phenyl), 7.68–7.73 (t, 3H) and 7.60 (s, 1H, bridging phenyl-C_2, C_3, C_5, C_6–H), 7.03–7.05 (d, J = 8 Hz, 1H, –CH pyrimidine), 6.60–6.74 (d, 2H, pyrrole-C_1, C_5–H), 6.32 (s, 4H, pyrrole-C_2, C $_4$–H), 5.22–5 (s, 2H, NH_2), 3.46 (s, 3H, OCH_3). ^{13}C NMR (100 MHz, DMSO-d_6) δ 164.89, 164.34, 164.07, 161.71, 130.57, 130.36, 128.81, 119.54, 119.43, 119.34, 119.19, 118.92, 111.95, 111.40. MS (ESI): m/z = found (M^+ + 1) 359.12, calc. 358.14. Anal. calcd. for $C_{21}H_{18}N_4O_2$: C, 70.38; H, 5.06; N, 15.63. Found: C, 70.40; H, 5.09; N, 15.66.

5.2.21 2-(6-(4-(1*H*-Pyrrol-1-yl)phenyl)-2-aminopyrimidin-4-yl)-6-methoxyphenol (4u). (Yield 85%). mp 180–181 °C; FTIR (KBr): 3359.20 cm^{-1} (NH_2), cm^{-1} (Ar–C=O), 1573.74 cm^{-1} (Ar C=C). ^1H NMR (400 MHz, DMSO-d_6) δ 14.25 (s, 1H, OH), 8.33–8.35 (d, J = 8.4 Hz, 2H) and 7.82–7.83 (d, J = 6.0 Hz, 2H, Ar-phenyl), 7.74–7.76 (d, J = 8.4 Hz, 2H), 7.51 (s, 1H–CH-pyrimidine), 7.22 (s, 2H, pyrrole-C_2, C_4–H), 7.06–7.08 (d, J = 8 Hz, 1H, –Ar phenyl) and 6.85–6.89 (s, 2H, NH_2), 6.32 (s, 2H, pyrrole-C_1, C_5–H), 3.46–3.81 (s, 3H, OCH_3 Benz). ^{13}C NMR (100 MHz, DMSO-d_6) δ 165.91, 164.85, 161.62, 151.41, 149.36, 142.10, 129.15, 119.99, 119.54, 119.46, 119.29, 118.93, 118.26, 117.90, 111.51, 100.31, 56.34. MS (ESI): m/z = found (M^+ + 1) 359.12, calc. 358.14. Anal. calcd. for $C_{21}H_{18}N_4O_2$: C, 70.38; H, 5.06; N, 15.63. Found: C, 70.42; H, 5.08; N, 15.66.

5.2.22 4-(4-(1*H*-Pyrrol-1-yl)phenyl)-6-(4-(dimethyl amino) styryl)pyrimidin-2-amine (4v). (Yield 80%). mp 168–169 °C; FTIR (KBr): 3318.39 cm^{-1} (NH_2), cm^{-1} (Ar–C=O), 1562.84 cm^{-1} (Ar C=C). ^1H NMR (400 MHz, DMSO-d_6) δ 8.19–8.21 (d, J = 8.0 Hz, 1H), 7.71–7.77 (t, 3H, CH=CH), 7.48–7.51 (t, 5H, pyrrole-C_2, C_4–H), 7.30 (s, 1H, –CH–pyrimidine), 6.74–6.76 (dd, J = 10.4 Hz, 4H, bridging phenyl-C_2, C_3, C_5, C_6–H), 6.48 (s, 1H, NH_2) and 6.28–6.31 (d, J = 12 Hz, 2H, pyrrole-C_1, C_5–H), 3.56–2.46 (s, 6H, 2CH_3). ^{13}C NMR (100 MHz, DMSO-d_6) δ 164.90.164.75, 163.42, 155.61, 148.26, 141.10, 128.75, 119.79, 119.64, 11.56, 119.38, 118.56, 117.80, 111.71, 100.31, 41.03. MS (ESI): m/z = found (M^+ + 1) 382.15, calc. 381.20. Anal. calcd. for $C_{24}H_{23}N_5$: C, 75.56; H, 6.08; N, 18.36. Found: C, 75.59; H, 6.12; N, 18.40.

5.3 ADMET, molecular docking, MMGBSA, DFT calculation & MD simulation

The crystal structures of Inha protein (PDB ID: 5OIR) from the PDB Database were used for docking studies. The InhA complexed protein structures were ready by Protein preparation wizard in Maestro Schrodinger Suite Release 2023-2 before performing docking. The absent hydrogens were added during the preparation and partial charges were given using OPLS-3E force field. Hydrogen and heavyweight atoms were minimized with constraints. Two-dimensional assemblies of 34 ligands with standard drugs prepared using Ligprep module in Maestro Schrodinger. With regard to this, Ligprep controls the protonation, and ionization conditions of the ligands, and given suitable bond commands.

Acceptable ADMET profile with effectiveness of the most important benchmarks for the conclusion of a drug. Found possible chalcone and pyrimidine derivatives based on molecular docking study. Further selected for *In silico* ADMET prediction to check its draggability using QikProp module in Schrodinger. The results are shown in (Table 1).

Docking 3D in addition 2D pose of highest anti-tubercular activity showing compound **4g** and involving the interaction with essential amino acids showing in (Fig. 7). Remaining compound showing better antitubercular activity glide docking score data and 2D, 3D images have been attached in ESI file.† The docking glide score shown in (Table 2).

The MMGBSA technique is a popular way to calculate a ligand's binding free energy to proteins or other macromolecules. It makes docking more efficient. Binding free energy calculate by the Prime module in Schrodinger software. For certain targets, MM-GBSA rescoring can be used to rank inhibitors and determine the proper binding poses score shown in (Table 3).

Schrodinger software's quantum physics suite, especially (Jaguar module), which is the company's tool for modelling electronic structures and quantum mechanics, may be used to do (DFT) computations and this module used for study the motion of electrons in atoms and molecules. It's based on the idea that the energy of a system is a function of its electron density, energy difference between the HOMO LUMO showed in (Table 8). After those molecular dynamics simulation was done (Desmond module of Schrodinger, LLC, New York, NY, version 2023-3). Molecular dynamics simulation was performed using Desmond module of Schrodinger suite (Desmond, Schrödinger, LLC, New York, NY, 2017). Performing MD simulation using OPLS4 forcefield. Molecular system was placed in an orthorhombic box in such a way that a buffer region of 10 Å was maintained between protein atoms and boundaries of the box. TIP3P water molecules was used to solvate the system and it is neutralized by adding 25 Na^+ and 17 Cl^- ions. The system was minimized and subjected to 200 ns MD simulation with NPT ensemble at 300 K temperature and 1.013 bar pressure while keeping other settings to their default values. In the MD simulation, a time step of 2 fs was used, while the energy and trajectory coordinates were recorded for every 5 ps. Maestro was used for analysing trajectories and calculating RMSDs from initial structures.

5.4 Biological activity

5.4.1 *In vitro* evaluation of antitubercular studies. The antitubercular potential of the synthesized compounds was assessed using the microplate alamar blue assay (MABA) against *Mycobacterium tuberculosis* H37Rv strain, following standard procedures.[50] Briefly, the bacterial inoculum was prepared by resuspending freshly cultured colonies in 7H9–S medium (containing 7H9 broth, 0.1% casitone, 0.5% glycerol, and OADC supplement), diluted 1 : 20, and adjusted to an OD590 of 1.0. Stock solutions of the test compounds were serially diluted in 7H9-S medium to achieve two-fold concentration gradients in 96-well microtiter plates. Each plate included a sterility control, a growth control without drug, and wells containing the test compounds. To minimize evaporation, sterile water was added to peripheral wells. Plates were sealed and incubated at 37 °C for 7 days. Afterward, 30 μL of Alamar Blue reagent was added to each well and plates were further incubated overnight. A color change from blue to pink indicated bacterial growth, and the minimum inhibitory concentration (MIC) was defined as the lowest concentration of the compound that prevented this color shift.[51]

5.4.2 Cytotoxicity MTT assay

5.4.2.1 MTT-based cytotoxicity activity on normal cell line. Cytotoxicity was evaluated using the RAW 264.7 mouse macrophage cell line (Mouse macrophage cell line (RAW 264.7) procured from BITS-Pilani Hyderabad campus itself) at a test concentration of 50 μg mL^{-1}. Cell viability was determined *via* the MTT assay, based on mitochondrial reduction of MTT to formazan after 48 hours of exposure. Cells were cultured in T25 flasks with RPMI medium containing 10% fetal bovine serum (FBS), (FBS was purchased from gibco, Thermo Fisher Scientific, USA). And 10 000 U per mL penicillin, and 10 mg per mL streptomycin, until they reached 80–90% confluency. Approximately 5000 cells were seeded per well in poly-L-lysine-coated 96-well plates and pre-incubated for 24 hours at 37 °C with 5% CO_2 and 100% humidity. Test compounds were then added, and the cells were incubated for an additional 48 hours. Subsequently, 10 μL of MTT solution (0.5 mg mL^{-1}) was added to each well, followed by 3 hours of incubation. The resulting formazan crystals were quantified by measuring absorbance at 595 nm and 625 nm.[52,53] Cytotoxicity on mouse macrophage cell line RAW 264.7 of the synthesized compounds was carried out at Birla Institute of Technology and Science-Pilani, Hyderabad Campus, Jawahar Nagar, Hyderabad, Telangana, India. Cytotoxicity assay was performed under standard protocols by Jyothi Kumari, Dharmarajan Sriram.

5.4.2.2 MTT-based cytotoxicity activity on lung cancer cell line. The MTT assay is a colorimetric method that uses the reduction of the yellow dissolved in water tetrazolium dye to formazan crystals to measure cell growth and cytotoxicity. MTT is reduced to insoluble formazan crystals by mitochondrial lactate dehydrogenase, which is produced by living cells. Crystals dissolve in an appropriate solvent and show a purple blue, the intensity of which is related to volume of viable cells and detected by spectrometer at 570 nm.[54,55] Lung Cancer cells procured from NCCS, Pune, India.

5.5 Enzyme inhibition studies

Sigma Aldrich provided the triclosan and NADH. The chosen compounds' stock solutions were made in DMSO so that, for all kinetic processes, the co-solvent's final concentration remained constant at 5% (v/v) in a final volume of 1 mL. As previously mentioned, *trans*-2-dodecenoyl-coenzyme A (DDCoA) and naturally occurring the protein InhA were used in kinetic tests. In summary, reactions were carried out at 25 °C in a buffer composed of water (30 mM PIPES (piperazine-*N*,*N*′-bis(2-ethanesulfonic acid)) and 150 mM NaCl pH 6.8) that included the test chemical (at 50 mM), 250 mM cofactor (NADH), and 50 mM substrate (DDCoA). InhA (final concentration of 100 nM) was added to start the reactions, and the oxidation of NADH was observed at a constant wavelength of 340 nm.[56] The % of inhibition of InhA activity (the reaction's starting velocity) relative to control the reaction without an inhibitor was used to indicate the activity of each selected derivative.

Abbreviations

ADME	Absorption, distribution, metabolism, and excretion
Ar	Aromatic
B3LYP	Becke, 3-parameter, Lee–Yang–Parr
d	Doublet
DDCoA	*Trans*-2-dodecenoyl-coenzyme A
DFT	Density functional theory
DMSO	Dimethyl sulfoxide
DNA	Deoxyribonucleic acid
DprE1	Decaprenyl phosphoryl-β-D-ribose 2′-epimerase
FAS	Fatty acid synthesis
FBS	Fetal bovine serum

HOMO	Highest occupied molecular orbital
INH	Isoniazid
IR	Infra-red
KAT	G enzyme catalase-peroxidase
LUMO	Lowest unoccupied molecular orbital
m	Multiplate
MD	Molecular dynamic
MDR	TB multidrug-resistant tuberculosis
MIC	Minimum inhibitory concentration
MM/GBSA	Molecular mechanics with generalized born and surface area
MS	Mass spectra
MTT	3-(4,5-Dimethylthiazol-2-yl)-2,5-diphenyltetrazolium bromide assay
NAD	Nicotinamide adenine dinucleotide
NMR	Nuclear magnetic resonance
NTM	Non-tuberculosis mycobacterial
OPLS-AA	Optimized potentials for liquid simulations in all atom version
PIPES	Piperazine-*N*,*N*′-bis(2-ethanesulfonic acid)
q	quadrate
RMSD	Root mean square deviation
RMSF	Root mean square fluctuation
RPMI	Roswell Park Memorial Institute Medium
TB	Tuberculosis
TIP 3P	Transferable intermolecular potential with 3 points
TLC	Thin-layer chromatography
TMS	Tetramethyl silane
vdW	Van der Waals
WHO	World health organization
XDR	TB extensively drug-resistant tuberculosis

Data availability

The ESI† contain the spectral data, *in silico* ESI† and biological activity data.

Author contributions

Deepshikha Singh: writing – review & editing, writing – original draft, software, resources, methodology, investigation, data curation, conceptualization, funding acquisition. Praveen M. Parkali: methodology & editing. Umme Hani, Riyaz Ali M. Osmani, Nazima Haider: visualization and formal analysis. Jyothi Kumari: performed anti-tubercular activity (MABA assay). Dharmarajan Sriram: supervision of *anti*-Tb activity and cytotoxicity assay. Christian Lherbet: provided INHA enzyme inhibition activity. Sheshagiri R. Dixit: conceptualization, supervision, validation, review & editing.

Conflicts of interest and competing interest

The authors declare no financial conflicts of interest or personal affiliations that could have influenced the research conducted in this study or any kind of conflict of interest. The authors declare the following financial interests/personal relationships which may be considered as potential competing interests. An Indian patent entitled "Synthetic strategies: methods for producing pyrimidine as anti-tubercular agent" has been granted related to this work (Indian Patent No. 568101 granted on 30th June-2025).

Acknowledgements

This research work was funded by Department of Science and Technology (DST), New Delhi by conferring the award of DST-WOMEN SCIENTIST Fellowship & Grant *via* DST Sanction Order No. DST-WOS-A (File No.: CS-13/WOS-A/2021) as financial support. The authors are thankful to the Management and Authorities of JSS Academy of Higher Education and Research (JSS AHER), Mysuru, India, for providing all computer aided drug design laboratory facilities. Authors also express gratitude to Mr Parthasarathi S., Analyst USIC, JSS College of Pharmacy, Mysuru, and the Director of SAIF, Karnataka University, Dharwad, and Vijnana Bhawan Mysore University, Mysuru, Karnataka, India, who have provided some of the NMR and mass spectral data. The authors extend their appreciation to the Deanship of Scientific Research at King Khalid University for funding this work through a Large Group Research Project under grant number RGP.2/259/46. The biological activity (cytotoxicity on A549 human lung cancer cell line) was carried out at Averin Biotech Labs, Bangalore, India and cytotoxicity assay was performed under standard protocols by Shiva Shankar Reddy G.

References

1 G. B. Migliori, C. W. M. Ong, L. Petrone, L. D'ambrosio, R. Centis and D. Goletti, The definition of tuberculosis infection based on the spectrum of tuberculosis disease, *Breathe*, 2021, **17**(3), 210079, DOI: **10.1183/20734735.0079-2021**.

2 Report GT, *WHO Reports Alarming Rise in Tuberculosis Cases in 2023*, 2024, pp. 2021–2023.

3 R. Villar-Hernández, A. Ghodousi, O. Konstantynovska, R. Duarte, C. Lange and M. Raviglione, Tuberculosis: current challenges and beyond, *Breathe*, 2023, **19**(1), 220166, DOI: **10.1183/20734735.0166-2022**.

4 *Global tuberculosis report 2024 by World Health Organization – Books on Google Play*, n.d., **https://play.google.com/store/books/details?id=cPwuEQAAQBAJ&rdid=book-cPwuEQAAQBAJ&rdot=1&source=gbs_vpt_read&pcampaignid=books_booksearch_viewport**, accessed December 19, 2024.

5 V. A. Dartois and E. J. Rubin, Anti-tuberculosis treatment strategies and drug development: challenges and priorities, *Nat. Rev. Microbiol.*, 2022, **20**(11), 685–701, DOI: **10.1038/s41579-022-00731-y**.

6 D. Singh, V. Singh, S. P. Mandal, K. Dsouza, B. R. P. Kumar and S. R. Dixit, Drug targets, current and future therapeutics for the treatment of multi drug resistant tuberculosis with their clinical applications: a critical review, *Curr. Drug Ther.*, 2024, **19**, 317–326, DOI: **10.2174/1574885519666230830125139**.

7 A. N. Unissa, S. Subbian, L. E. Hanna and N. Selvakumar, Overview on mechanisms of isoniazid action and resistance in *Mycobacterium tuberculosis*, *Infect. Genet. Evol.*, 2016, **45**, 474–492, DOI: 10.1016/J.MEEGID.2016.09.004.

8 S. L. Parikh, G. Xiao and P. J. Tonge, Inhibition of InhA, the enoyl reductase from *Mycobacterium tuberculosis*, by triclosan and isoniazid, *Biochemistry*, 2000, **39**, 7645–7650, DOI: 10.1021/BI0008940.

9 K. Rožman, I. Sosič, R. Fernandez, R. J. Young, A. Mendoza, S. Gobec, *et al.*, A new "golden age" for the antitubercular target InhA, *Drug Discov. Today*, 2017, **22**, 492–502, DOI: 10.1016/J.DRUDIS.2016.09.009.

10 P. Kamsri, N. Koohatammakun, A. Srisupan, P. Meewong, A. Punkvang, P. Saparpakorn, *et al.*, Rational design of InhA inhibitors in the class of diphenyl ether derivatives as potential anti-tubercular agents using molecular dynamics simulations, *SAR QSAR Environ. Res.*, 2014, **25**, 473–488, DOI: 10.1080/1062936X.2014.898690.

11 M. E. Boyne, T. J. Sullivan, C. W. AmEnde, H. Lu, V. Gruppo, D. Heaslip, *et al.*, Targeting fatty acid biosynthesis for the development of novel chemotherapeutics against Mycobacterium tuberculosis: evaluation of A-ring-modified diphenyl ethers as high-affinity InhA inhibitors, *Antimicrob. Agents Chemother.*, 2007, **51**, 3562–3567, DOI: 10.1128/AAC.00383-07.

12 X. He, A. Alian and P. R. Ortiz de Montellano, Inhibition of the *Mycobacterium tuberculosis* enoyl acyl carrier protein reductase InhA by arylamides, *Bioorg. Med. Chem.*, 2007, **15**, 6649–6658, DOI: 10.1016/J.BMC.2007.08.013.

13 X. He, A. Alian, R. Stroud and P. R. Ortiz De Montellano, Pyrrolidine carboxamides as a novel class of inhibitors of enoyl acyl carrier protein reductase from *Mycobacterium tuberculosis*, *J. Med. Chem.*, 2006, **49**, 6308–6323, DOI: 10.1021/JM060715Y.

14 U. H. Manjunatha, S. P. S. Rao, R. R. Kondreddi, C. G. Noble, L. R. Camacho, B. H. Tan, *et al.*, Direct inhibitors of InhA active against *Mycobacterium tuberculosis*, *Sci. Transl. Med.*, 2015, **7**, 269ra3, DOI: 10.1126/SCITRANSLMED.3010597.

15 B. Ardiansah, Chalcones bearing N, O, and S-heterocycles: recent notes on their biological significances, *J. Appl. Pharm. Sci.*, 2019, **9**, 117–129, DOI: 10.7324/JAPS.2019.90816.

16 A. Bavishi, H. Vala, A. Radadiya, S. Swami, S. Thakrar, D. Sarkar, *et al.*, Synthesis, biological screening, and molecular docking of hybrid pyrazole scaffolds for antitubercular and antimicrobial activity, *ChemistrySelect*, 2025, **10**, e202404830, DOI: 10.1002/SLCT.202404830.

17 A. Yadav, V. Sharma and G. Singh, Anti-inflammatory potential of chalcone related compounds: an updated review, *ChemistrySelect*, 2024, **9**, e202401321, DOI: 10.1002/SLCT.202401321.

18 B. Chaithanya, D. P. Chary and V. R. Anna, Synthesis and biological evaluation of chalcone incorporated thaizole-isoxazole derivatives as anticancer agents, *Chem. Data Collect.*, 2025, **55**, 101177, DOI: 10.1016/J.CDC.2024.101177.

19 C. X. yin, Z. Z. jia, X. J. lin, M. Yang and Z. Wang, Experimental and molecular docking studies of estrogen-like and anti-osteoporosis activity of compounds in Fructus Psoraleae, *J. Ethnopharmacol.*, 2021, **276**, 114044, DOI: 10.1016/J.JEP.2021.114044.

20 D. U. Dave, H. Patel, N. C. Bhoraniya, P. Pankhaniya and D. M. Purohit, Synthesis, spectral studies and antimicrobial screening of some new chalcone and isoxazole derivatives bearing furan nucleus, *World J. Pharm. Res.*, 2024, **13**(12), 747–756, DOI: 10.20959/wjpr202412-32783.

21 R. Gaur, K. S. Jyoti, H. S. Cheema, F. Khan, M. P. Darokar, *et al.*, Synthesis, molecular modelling studies of artemisinin-chalcone derivatives and their antimalarial activity evaluation, *Nat. Prod. Res.*, 2024, 1–11, DOI: 10.1080/14786419.2024.2375784.

22 D. Elkhalifa, I. Al-Hashimi, A. E. Al Moustafa and A. Khalil, A comprehensive review on the antiviral activities of chalcones, *J. Drug Target.*, 2021, **29**, 403–419, DOI: 10.1080/1061186X.2020.1853759.

23 R. Segawa, H. Takeda, T. Yokoyama, M. Ishida, C. Miyata, T. Saito, *et al.*, A chalcone derivative suppresses TSLP induction in mice and human keratinocytes through binding to BET family proteins, *Biochem. Pharmacol.*, 2021, **194**, 114819, DOI: 10.1016/J.BCP.2021.114819.

24 R. C. Choudhari, K. Kaur, A. Das and V. Jaitak, Synthesis, and in-silico studies of indole-chalcone derivatives targeting estrogen receptor alpha (ER-α) for breast cancer, *Curr. Comput. Aided Drug Des.*, 2023, **20**, 640–652, DOI: 10.2174/0115734099263650230926053750.

25 M. N. Gomes, E. N. Muratov, M. Pereira, J. C. Peixoto, L. P. Rosseto, P. V. L. Cravo, *et al.*, Chalcone derivatives: promising starting points for drug design, *Molecules*, 2017, **22**(8), 1210, DOI: 10.3390/molecules22081210.

26 N. Jeelan Basha and K. T. Akshay, Design, synthesis, drug-likeness, anti-inflammatory, antimicrobial activity, and molecular docking studies of pyrimidine analogs, *Polycyclic. Aromat. Compd.*, 2024, **24**(10), 6957–6969, DOI: 10.1080/10406638.2024.2331519.

27 W. Shehta, N. A. Alsaiari, B. Farag, M. M. Abdel-Aziz, S. Youssif, S. El-Kalyoubi, *et al.*, Novel phthalimide-pyrimidine hybrids as potent anti-tubercular agents, 2024, DOI: 10.21203/rs.3.rs-4397392/v1.

28 M. S. Raghu, C. B. Pradeep Kumar, K. Yogesh Kumar, M. K. Prashanth, F. Alharethy and B. H. Jeon, Synthesis, biological evaluation and molecular docking study of pyrimidine linked thiazolidinedione derivatives as potential antimicrobial and antitubercular agents, *Bioorg. Med. Chem. Lett.*, 2024, **103**, 129707, DOI: 10.1016/j.bmcl.2024.129707.

29 A. Bhatnagar and G. Pemawat, Anticancer and antibacterial activeness of fused pyrimidines: newfangled updates, *Bioorg. Chem.*, 2024, **153**, 107780, DOI: 10.1016/J.BIOORG.2024.107780.

30 H. Kaur, L. Singh, K. Chibale and K. Singh, Structure elaboration of isoniazid: synthesis, *in silico* molecular docking and antimycobacterial activity of isoniazid–pyrimidine conjugates, *Mol. Divers.*, 2020, **24**, 949–955, DOI: 10.1007/S11030-019-10004-1/METRICS.

31 M. Y. Lone, M. Athar, V. K. Gupta and P. C. Jha, Identification of *Mycobacterium tuberculosis* enoyl-acyl carrier protein reductase inhibitors: a combined *in silico* and *in vitro* analysis, *J. Mol. Graph. Model.*, 2017, **76**, 172–180, DOI: 10.1016/J.JMGM.2017.07.005.

32 S. Chinnamulagund, A. S. Joshi, S. Avunoori, V. H. Kulkarni, S. D. Joshi and C. D. Shrinivas Joshi Professor, Synthesis and antitubercular evaluation of certain pyrrole derivatives, *Indo Am. J. Pharm. Res.*, 2023, **13**(03), DOI: 10.5281/zenodo.7755252.

33 F. Cerreto, A. Villa, A. Retico and M. Scalzo, Studies on anti-candida agents with a pyrrole moiety. Synthesis and microbiological activity of some 3-aminomethyl-1,5-diaryl-2-methyl-pyrrole derivatives, *Eur. J. Med. Chem.*, 1992, **27**, 701–708, DOI: 10.1016/0223-5234(92)90090-N.

34 D. Deidda, G. Lampis, R. Fioravanti, M. Biava, G. C. Porretta, S. Zanetti, *et al.*, Bactericidal activities of the pyrrole derivative BM212 against multidrug-resistant and intramacrophagic *Mycobacterium tuberculosis* strains, *Antimicrob. Agents Chemother.*, 1998, **42**, 3035–3037, DOI: 10.1128/AAC.42.11.3035.

35 R. Shah, P. K. Verma, M. Shah and S. Kumar, Design, synthesis, biological evaluation and molecular docking studies of thiophene derivatives, *J. Iran. Chem. Soc.*, 2024, **21**, 2501–2515, DOI: 10.1007/S13738-024-03088-6/FIGURES/9.

36 G. Dheeraj, P. Kumar, K. Apte, H. Ashtekar and S. R. Dixit, Molecular docking, ADME analysis, and pharmacophore modelling of benzoxazole fused azetidinone derivatives as antibreast cancer agents, *Ann. Phytomed. Int. J.*, 2023, **12**(1), 318–324, DOI: 10.54085/AP.2023.12.1.37.

37 A. Fatima, G. Khanum, S. K. Srivastava, P. Bhattacharya, A. Ali, H. Arora, *et al.*, Exploring quantum computational, molecular docking, and molecular dynamics simulation with MMGBSA studies of ethyl-2-amino-4-methyl thiophene-3-carboxylate, *J. Biomol. Struct. Dyn.*, 2023, **41**, 10411–10429, DOI: 10.1080/07391102.2023.2180667.

38 M. Khanal, A. Acharya, R. Maharjan, K. Gyawali, R. Adhikari, M. D. Das, *et al.*, Identification of potent inhibitors of HDAC2 from herbal products for the treatment of colon cancer: molecular docking, molecular dynamics simulation, MM/GBSA calculations, DFT studies, and pharmacokinetic analysis, *PLoS ONE*, 2024, **19**, e0307501, DOI: 10.1371/JOURNAL.PONE.0307501.

39 M. I. Choudhary, M. Shaikh, M. Tul-Wahab and M. Ur-Rahman, *In silico* identification of potential inhibitors of key SARS-CoV-2 3CL hydrolase (Mpro) *via* molecular docking, MMGBSA predictive binding energy calculations, and molecular dynamics simulation, *PLoS One*, 2020, **15**, e0235030, DOI: 10.1371/journal.pone.0235030.

40 S. Jain, S. Sharma and D. J. Sen, Virtual screening, docking, ADMET and molecular dynamics: a study to find novel inhibitors of mycobacterium tuberculosis targeting QcrB, *Jordan J. Chem. (JJC)*, 2021, **16**, 131–146, DOI: 10.47014/16.3.4.

41 I. Ahmad, H. Jadhav, Y. Shinde, V. Jagtap, R. Girase and H. Patel, Optimizing bedaquiline for cardiotoxicity by structure based virtual screening, DFT analysis and molecular dynamic simulation studies to identify selective MDR-TB inhibitors, *In Silico Pharmacol.*, 2021, **9**(1), 23, DOI: 10.1007/S40203-021-00086-X.

42 D. Panigrahi and S. K. Sahu, Computational approaches: atom-based 3D-QSAR, molecular docking, ADME-Tox, MD simulation and DFT to find novel multi-targeted anti-tubercular agents, *BMC Chem.*, 2025, **19**, 39, DOI: 10.1186/S13065-024-01357-2.

43 A. Krishnan, F. I. Khan, S. Sukumar and M. K. A. Khan, Identification of potential molecular targets and repurposed drugs for tuberculosis using network-based screening approach, molecular docking, and simulation, *J. Biomol. Struct. Dyn.*, 2025, **43**(1), 73–91, DOI: 10.1080/07391102.2023.2279699.

44 S. Thapa, M. S. Biradar, S. L. Nargund, I. Ahmad, M. Agrawal, H. Patel, *et al.*, Synthesis, molecular docking, molecular dynamic simulation studies, and antitubercular activity evaluation of substituted benzimidazole derivatives, *Adv. Pharmacol. Pharm. Sci.*, 2024, **2024**, 9986613, DOI: 10.1155/2024/9986613.

45 I. Pauli, R. N. Dos Santos, D. C. Rostirolla, L. K. Martinelli, R. G. Ducati, L. F. S. M. Timmers, *et al.*, Discovery of new inhibitors of *Mycobacterium tuberculosis* InhA enzyme using virtual screening and a 3D-pharmacophore-based approach, *J. Chem. Inf. Model.*, 2013, **53**, 2390–2401, DOI: 10.1021/CI400202T.

46 A. Chollet, L. Maveyraud, C. Lherbet and V. Bernardes-Génisson, An overview on crystal structures of InhA protein: apo-form, in complex with its natural ligands and inhibitors, *Eur. J. Med. Chem.*, 2018, **146**, 318–343, DOI: 10.1016/J.EJMECH.2018.01.047.

47 F. Prati, F. Zuccotto, D. Fletcher, M. A. Convery, R. Fernandez-Menendez, R. Bates, *et al.*, Screening of a novel fragment library with functional complexity against *Mycobacterium tuberculosis* InhA, *ChemMedChem*, 2018, **13**, 672–677, DOI: 10.1002/CMDC.201700774.

48 A. Hospital, J. R. Goñi, M. Orozco and J. L. Gelpí, Molecular dynamics simulations: advances and applications, *Adv. Appl. Bioinform. Chem.*, 2015, **8**, 37, DOI: 10.2147/AABC.S70333.

49 S. D. Joshi, S. R. Dixit, M. N. Kirankumar, T. M. Aminabhavi, K. V. S. N. Raju, R. Narayan, *et al.*, Synthesis, antimycobacterial screening and ligand-based molecular docking studies on novel pyrrole derivatives bearing pyrazoline, isoxazole and phenyl thiourea moieties, *Eur. J. Med. Chem.*, 2016, **107**, 133–152, DOI: 10.1016/J.EJMECH.2015.10.047.

50 S. Sahana, G. R. Vijayakumar, R. Sivakumar, D. Sriram and D. V. Saiprasad, Synthesis, docking study and *in vitro* evaluation of anti-tuberculosis activity of tri substituted imidazoles containing quinoline moiety, *J. Korean Chem. Soc.*, 2022, **66**, 194–201, DOI: 10.5012/JKCS.2022.66.3.194.

51 L. A. Collins and S. G. Franzblau, Microplate alamar blue assay *versus* BACTEC 460 system for high-throughput screening of compounds against *Mycobacterium tuberculosis* and *Mycobacterium avium*, *Antimicrob. Agents*

Chemother., 1997, **41**, 1004–1009, DOI: **10.1128/AAC.41.5.1004**.

52 T. M. Dhameliya, K. I. Patel, R. Tiwari, S. K. Vagolu, D. Panda, D. Sriram, *et al.*, Design, synthesis, and biological evaluation of benzo[d]imidazole-2-carboxamides as new anti-TB agents, *Bioorg. Chem.*, 2021, **107**, 104538, DOI: **10.1016/J.BIOORG.2020.104538**.

53 T. Mosmann, Rapid colorimetric assay for cellular growth and survival: application to proliferation and cytotoxicity assays, *J. Immunol. Methods*, 1983, **65**, 55–63, DOI: **10.1016/0022-1759(83)90303-4**.

54 C. M. Tsai, R. P. Perng, K. T. Chang, D. Venzon and A. F. Gazdar, Evaluation of the relative cytotoxic effects of anticancer agents in serum-supplemented *versus* serum-free media using a tetrazolium colorimetric assay, *Jpn. J. Cancer Res.*, 1996, **87**, 91–97, DOI: **10.1111/j.1349-7006.1996.tb00205.x**.

55 P. Hoffmann, J. Azéma-Despeyroux, F. Goncalves, A. Stamilla, N. Saffon-Merceron, F. Rodriguez, *et al.*, Imidazoquinoline derivatives as potential inhibitors of InhA enzyme and *Mycobacterium tuberculosis*, *Molecules*, 2024, **29**, 3076, DOI: **10.3390/MOLECULES29133076/S1**.

56 S. D. Joshi, S. R. Dixit, J. Basha, V. H. Kulkarni, T. M. Aminabhavi, M. N. Nadagouda, *et al.*, Pharmacophore mapping, molecular docking, chemical synthesis of some novel pyrrolyl benzamide derivatives and evaluation of their inhibitory activity against enoyl-ACP reductase (InhA) and *Mycobacterium tuberculosis*, *Bioorg. Chem.*, 2018, **81**, 440–453, DOI: **10.1016/J.BIOORG.2018.08.035**.